

# Textural trends in turbidites and slurry beds from the Oligocene flysch of the East Carpathians, Romania

ZOLTÁN SYLVESTER<sup>1</sup> and DONALD R. LOWE

*Department of Geological and Environmental Sciences, Stanford University, Stanford, CA 94305-2115, USA*

## ABSTRACT

Deep-water sandstone beds of the Oligocene Fusaru Sandstone and Lower Dysodilic Shale, exposed in the Buzău Valley area of the East Carpathian flysch belt, Romania, can be described in terms of the standard turbidite divisions. In addition, mud-rich sand layers are common, both as parts of otherwise 'normal' sequences of turbidite divisions and as individual event beds. Eleven units, interpreted as the deposits of individual flows, were densely sampled, and 87 thin sections were point counted for grain size and mud content.  $S_3/T_a$  divisions, which form the bulk of most sedimentation units, have low internal textural variability but show subtle vertical trends in grain size. Most commonly, coarse-tail normal grading is associated with fine-tail inverse grading. The mean grain size can show inverse grading, normal grading or a lack of grading, but sorting tends to improve upward in most beds. Fine-tail inverse grading is interpreted as resulting from a decreasing effectiveness of trapping of fines during rapid deposition from a turbidity current as the initially high suspended-load fallout rate declines. If this effect is strong enough, the mean grain size can show subtle inverse grading as well. Thus, thick inversely graded intervals in deep-water sands lacking traction structures do not necessarily imply waxing flow velocities. If the suspended-load fallout rate drops to zero after the deposition of the coarse grain-size populations, the remaining finer grained flow bypasses and may rework the top of the  $S_3$  division, forming well-sorted, coarser grained, current-structured  $T_1$  units. Alternatively, the suspended-load fallout rate may remain high enough to prevent segregation of fines, leading to the deposition of significant amounts of mud along with the sand. Mud content of the sandstones is bimodal: either 3–13% or more than 20%. Two types of mud-rich sandstones were observed. Coarser grained mud-rich sandstones occur towards the upper parts of  $S_3/T_a$  divisions. These units were deposited as a result of enhanced trapping of mud particles in the rapidly deposited sediment. Finer grained mud-rich units are interbedded with ripple-laminated very fine-grained sandy  $T_c$  divisions. During deposition of these units, mud floccules were hydraulically equivalent to the very fine sand- and silt-sized sediment. The mud-rich sandstones were probably deposited by flows that became transitional between turbidity currents and debris flows during their late-stage evolution.

**Keywords** Debris flows, East Carpathians, grading, grain-size distributions, inverse grading, turbidites.

<sup>1</sup>Present address: Shell International Exploration and Production Inc., 3737 Bellaire Blvd, PO Box 481, Houston, TX 77001-0481, USA (E-mail: zoltan.sylvester@shell.com)

## INTRODUCTION

Since the recognition that large volumes of siliciclastic sediment are transported into deep water

by sediment gravity flows (Kuenen & Migliorini, 1950), the textural characteristics of these deposits have been considered to be important indicators of flow hydrodynamics (Middleton, 1967; Kuenen & Sengupta, 1970; Lowe, 1982; Kranck, 1984; Komar, 1985). Normal size grading seems to be one of the characteristic features of turbidites (Kuenen & Migliorini, 1950; Middleton, 1993), and sorting is typically poorer than in shallow-marine or fluvial sediments (Kuenen & Menard, 1952; Hiscott, 1994a). The experiments of Middleton (1967) demonstrated that two types of normal grading were produced by rapid deposition from turbidity currents: coarse-tail and distribution grading. Distribution grading, involving a progressive fining of the entire grain-size spectrum, commonly characterizes the gradual transition from sand to mud through the Bouma T<sub>b</sub>, T<sub>c</sub>, T<sub>d</sub> and T<sub>e</sub> divisions. Coarse-tail grading, involving a decrease in only the coarser size grades, is common in thick S<sub>3</sub> (Lowe, 1982) or T<sub>a</sub> (Bouma, 1962) divisions of turbidites.

However, there is growing evidence that vertical textural trends in relatively thick sandy turbidites can be more complex. Middleton (1962) documented that the maximum grain size decreases upwards in turbidites of the Norman-skill and Charny Formations, but the mean grain size is 'not so simply a function of the hydrodynamics of the turbidity current as the maximum size'. Hiscott & Middleton (1980) observed that structureless deep-water sandstones are commonly poorly graded, ungraded or inverse-to-normally graded. Lowe (1982) has emphasized the role of 'fluctuations in the rate of suspended-load fallout' during deposition from high-density turbidity currents, which can result in complex structuring and grain-size trends in thick, coarse-grained, deep-water deposits. Some outcrop observations of massive sands seem to suggest a common lack of normal grading in such units, although it is difficult or impossible to detect subtle textural changes in finer grained sandstones without quantitative grain-size studies. Even where coarse-tail grading is visible in the outcrop as a result of the presence of granule- to pebble-grade material, quantitative grain-size studies are necessary to determine whether the remaining admixed finer sediment shows similar size trends.

Since the work of Middleton (1962), Gonzalez-Bonorino & Middleton (1976), Hiscott & Middleton (1979, 1980) and Taira & Scholle (1979), there have been few quantitative textural studies of deep-water sands lacking traction structures.

Although the alleged rarity of normal grading formed the starting point for both the sandy debris-flow debate, initiated by Shanmugam & Moiola (1995), and the quasi-steady current model of Kneller & Branney (1995), no quantitative textural data were provided to document the supposed lack of normal grading in the thick S<sub>3</sub> divisions that formed the basis of these discussions.

Inverse or more complex vertical grain-size trends are usually explained as reflecting the development of dispersive pressure and kinetic sieving in highly concentrated near-bed flow layers and variations on the traction carpet model (Lowe, 1982; Hiscott, 1994b; Sohn, 1997) or by changes in the mean velocity of the current. Examples of the latter include the acceleration matrix of Kneller (1995) and the model of coarse-sediment transport lag of Hand (1997). The traction carpet model fails to explain sandy inversely graded intervals that are thicker than a few centimetres (Lowe, 1976). Interpretations that relate changes in grain size directly to changes in flow velocity ignore the fact that: (1) there seems to be no simple relationship between mean grain size of the turbidite and mean flow velocity (Middleton, 1962; Komar, 1985); (2) turbidity currents that are depositing thick beds are probably overloaded with sediment, and resulting variations in sedimentation rate and flow concentration can be expected (Kuenen & Sengupta, 1970; Lowe, 1988; Allen, 1991; Hiscott, 1994a); and (3) only turbulence, not flow velocity, directly influences particle distribution in the flow (Felix, 2002).

In addition to size grading, the abundance and distribution of detrital mud is an important feature of sand-rich sediment gravity flow deposits that bears directly on their processes of deposition. It has long been recognized that the relatively high mud contents of many deep-water sands result from simultaneous and rapid deposition of most grain sizes present in suspension (Kuenen, 1966). Lowe & Guy (2000) and Lowe *et al.* (2003) described mud-rich sandstones in the Britannia Formation, North Sea, that show a distinctive assemblage of sedimentary structures suggesting deposition influenced by both grain-by-grain traction processes and cohesive particle interactions. These mud-rich beds have been interpreted as the deposits of slurry flows, flows transitional between turbidity currents and debris flows. Similar sedimentation units also exist in other formations (e.g. Hiscott & Middleton, 1979), but have not been well documented. Sandy

mudrocks and mud-rich sandstones associated with underlying structureless sandstones were described recently and interpreted as debrites related to cogenetic concentrated gravity currents by Haughton *et al.* (2003).

In this paper, the term 'turbidity current' is used for flows 'in which the sediment is supported mainly by the upward component of fluid turbulence' (Middleton & Hampton, 1976), and their inferred deposits are considered to be turbidites. Some of the event beds studied here suggest that a turbidity current can undergo significant transformations during its depositional stage and that parts or most of the resulting deposits may show signs of cohesive freezing. Therefore, if it can reasonably be inferred that the main transport mechanism must have been a turbidity current, the transporting sediment flow will not be called a debris flow. The terms 'slurry flow' and 'slurry bed' are used as defined in Lowe & Guy (2000).

This study focuses on deep-water sands of the Oligocene flysch of the East Carpathians, Romania. Outcrops of the Fusaru Sandstone include interbedded mud-poor turbidity current and mud-rich slurry-flow deposits. Layers of mud-rich sand occur not only as individual slurry-flow sedimentation units, but also as parts of units made up largely of mud-poor turbidite divisions of Bouma (1962) or Lowe (1982). The objectives of this paper are: (1) to document textural properties of thick-bedded mud-rich and mud-poor units of the Fusaru Sandstone and the Lower Dysodilic Shale; and (2) to use these textural features along with sedimentary structures to interpret the dynamics and late-stage evolution of the depositing flows.

## METHODS

### Grain-size measurements in thin sections

Two exposures of deep-water rocks of Oligocene age (A and B in Fig. 1b) were selected for study. Detailed stratigraphic sections were measured at the two localities to characterize the overall packaging within the successions. Bed thicknesses, sedimentary structures and maximum grain sizes in the coarser grained sedimentation units were among the observations made at the outcrops.

Mud-poor and mud-rich sandstone beds in sections A and B, covering a wide range of thicknesses and structures, were selected for

quantitative textural study. Those with complex internal structures were relogged at a scale of 1:10. Most beds were sampled at more than four points along a vertical section. Thin sections were cut perpendicular to bedding and essentially randomly oriented relative to flow direction. In total, 87 thin sections were point counted for grain size using a standard grid technique with an optical microscope and a digital point counting system that automatically records grain lengths on a computer. Only maximum grain diameters were recorded. Three hundred quartz and feldspar grain lengths were measured in each thin section. This number provides sufficient accuracy, even in poorly sorted sandstones (Johnson, 1994). For all thin sections, modal composition was determined as well, using the Gazzi–Dickinson point counting method. However, a detailed petrographic analysis of the rocks was not a major goal of this study. Mud content was determined as part of this modal count, based on optical petrographic criteria, rather than a fixed grain-size limit.

The measurement of grain size in thin sections has several limitations that need to be addressed (for a review, see Johnson, 1994). First, mean diameters in  $\phi$  units obtained in thin sections of spherical grains underestimate the real mean values by 0.2023  $\phi$  (Johnson, 1994). In this paper, the raw grain-size data are used; no corrections were applied to obtain the sieve or equivalent sphere diameter.

Secondly, the fine tail of the resulting distribution is affected by the resolution of the measurement technique. With the methodology and samples used in this paper, it was found that reasonable precision can be obtained down to a grain size of 5.5  $\phi$  ( $\approx$  0.02 mm). A similar lower limit was suggested by Johnson (1994) that is low enough to ensure that the resulting distributions are not significantly truncated.

Thirdly, the coarse tails of the measured distributions, especially in poorly sorted, coarser grained sandstones, are underestimated because of difficulties in obtaining representative thin-section samples of such sandstones with sparsely dispersed pebbles. Therefore, it might be problematic to quantify coarse-tail normal grading that seems obvious in the outcrop.

Descriptive statistical measures were derived from the data after conversion to the  $\phi$  scale. Measured  $\phi$  grain sizes are approximately normally distributed for all samples, suggesting a log-normal distribution for the data in millimetres. The mean grain size calculated on the  $\phi$

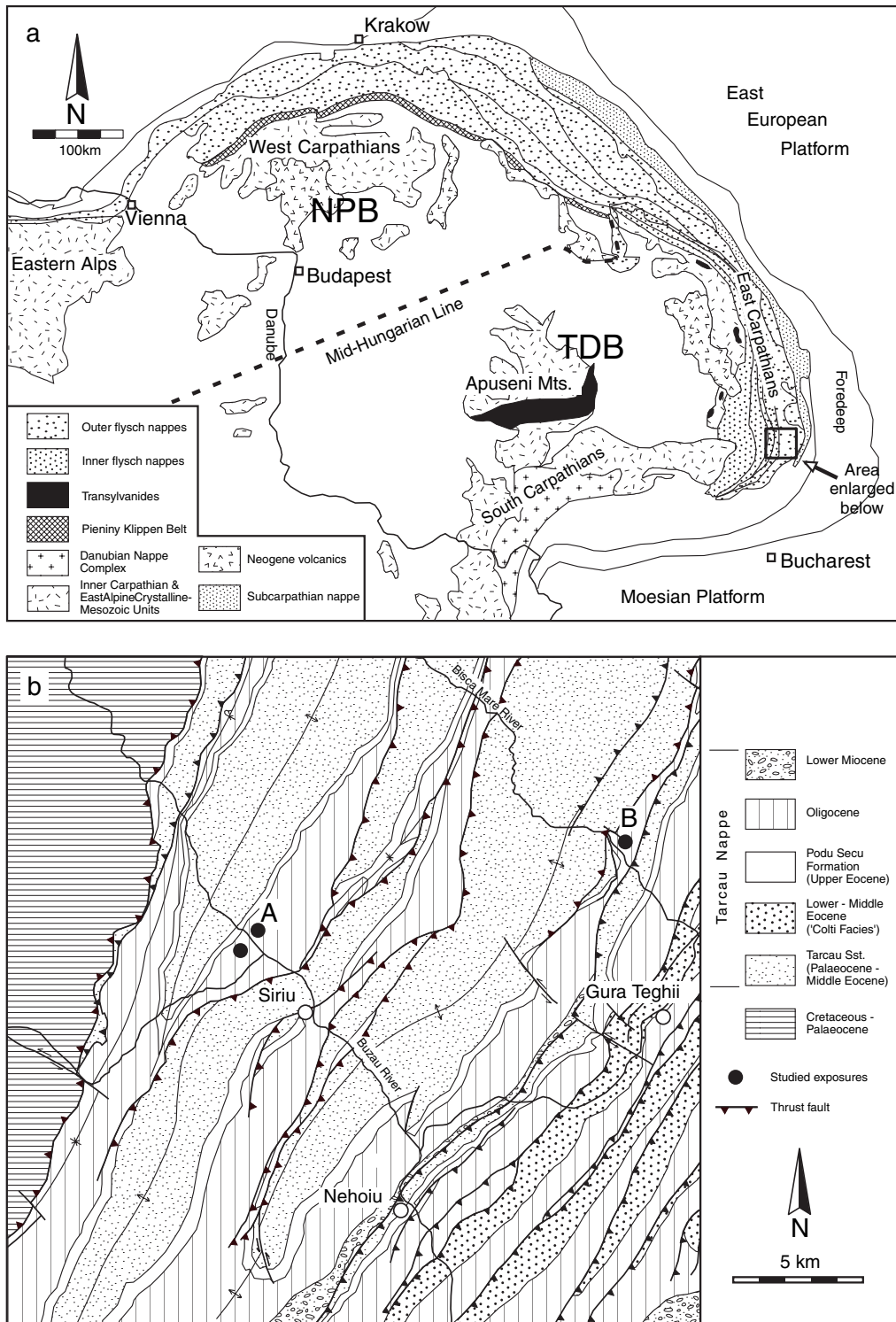


**Fig. 1.** (a) Geological sketch map of the Carpathians. The two intra-Carpathian continental blocks (TDB, Tisza-Dacia Block; NPB, North Pannonian Block) are separated by a large wrench fault zone, the Mid-Hungarian Line. (b) Detailed geological map of the Tarcău Nappe in the Buzău Valley area, with locations of studied exposures (A and B).

scale is a better measure of the central tendency than the arithmetic mean derived from the data in millimetres, and it corresponds to the geometric mean on the metric scale (Pierce &

Graus, 1981). Sediment sorting was estimated using  $\phi$  sorting, that is the standard deviation of the  $\phi$  distribution.  $\phi$  sorting as measured in thin sections has a minimum value of 0.284  $\phi$  in the

case of a sediment composed of identical spherical grains (Johnson, 1994). Error bars on the mean and the standard deviation were defined as the 95% confidence limits based on standard errors of the mean and the standard deviation respectively. The standard error of the mean is

$$\sigma_m = \sigma/\sqrt{n} \quad (1)$$

where  $\sigma$  is the standard deviation of the population and  $n$  is the number of counts; the standard error of the standard deviation is

$$\sigma_s = \sigma/\sqrt{(2n)} \quad (2)$$

The standard error of the standard deviation has a normal distribution only for a large number of samples, a condition that is met here, and it gives a rough guide to the precision of the standard deviation (e.g. Davies & Goldsmith, 1977).

### Statistical methodology for vertical grain-size trend analysis

A question that is rarely addressed in textural studies is whether the grain-size trends through beds and differences in grain size are statistically significant. A small difference in the mean grain size between two samples from the same bed cannot serve as evidence for grain-size trends. In many cases, the difference between two adjacent samples is so small that the null hypothesis of equal population means cannot be rejected. However, it is still possible that the subtle differences across several samples are consistent and show a statistically significant vertical trend. To reduce the subjectivity of assigning vertical grain-size trends, the statistical significance of these has been tested with trend analysis (e.g. Dean & Voss, 1999, p. 71). In this case, a test of the linear component of trend is a test of whether there is a significant decrease or increase in a grain-size parameter as a function of vertical position in the bed. In order to calculate significance levels for both the mean grain sizes and other statistics (standard deviation, fifth and 95th percentiles), a randomization method was applied. For the interval of interest, all the grain diameters were shuffled, and 1000 random sequences were generated through resampling with replacement. Significance levels ( $P$ -values) can then be calculated by comparing the linear component of trend in the real data set with the ones coming from the randomizations.

## GEOLOGICAL BACKGROUND

### Tectonic and stratigraphic setting

The flysch belt of the Romanian East Carpathians (Fig. 1a) consists of deep-water sediments of Late Jurassic to Miocene age that were deposited in a shrinking ocean basin. Tectonic and palaeomagnetic studies suggest that complicated translations, rotations and internal deformation of two microcontinents, the North Pannonian and the Tisza–Dacia blocks, influenced the evolution of the flysch basin (Fig. 2). The motions of the two blocks were constrained by the pre-existing large-scale structure of the East European passive continental margin in an overall compressional setting determined by the convergence of the Eurasian and African plates (Linzer *et al.*, 1998; Fodor *et al.*, 1999). The two blocks migrated from the west and south-west into an oceanic embayment on the East European margin (Fig. 2). The general northward-oriented palaeocurrent pattern suggests that the principal source area for the Palaeogene turbidite systems was not the inner, western part of the East Carpathian orogen; rather, the main sediment input points were at the southern end of the flysch belt (Contescu *et al.*, 1967). In addition, smaller deep-water systems developed along the eastern, passive side of the basin (= Kliwa depositional systems), with compositions and palaeocurrent patterns different from those closer to the active margin. During the Oligocene, two sand-rich formations were deposited: the Fusaru Sandstone, with a

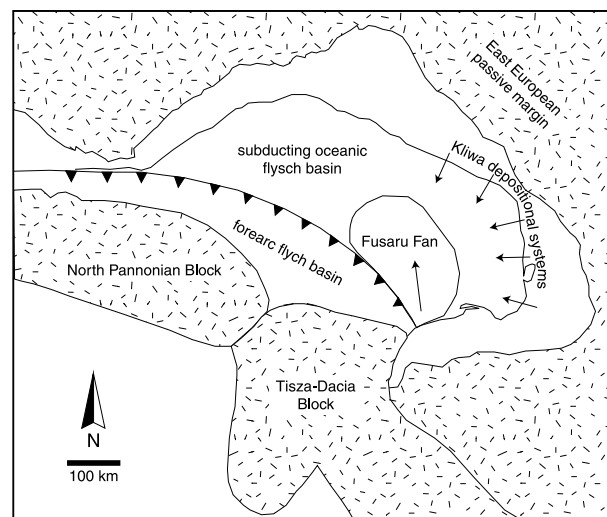


Fig. 2. Palaeogeographic sketch of the Alpine-Carpathian area during the Palaeogene. Modified from Fodor *et al.*, (1999).

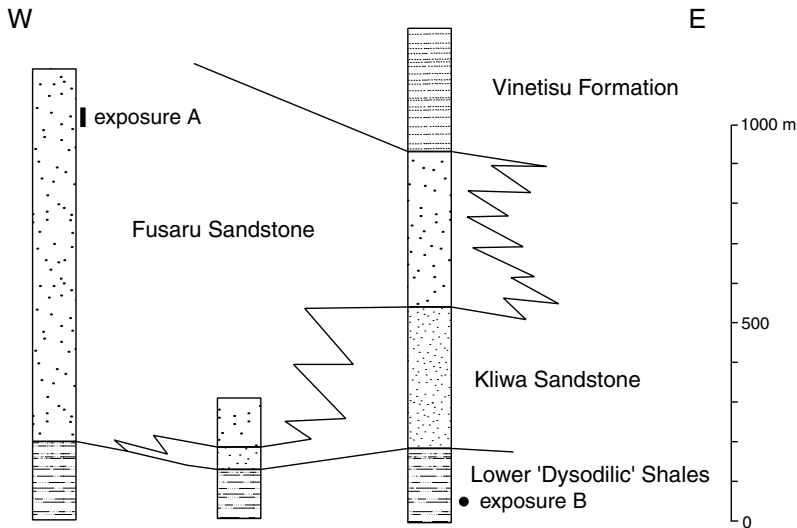


Fig. 3. Lithostratigraphy of Oligocene flysch deposits in the Buzău Valley area. Simplified from Ştefănescu *et al.* (1993).

northward palaeocurrent pattern and a quartzofeldspathic composition; and the Kliwa Sandstone, a quartz arenite with an eastern source area (Ştefănescu & Micu, 1987). Both of these are underlain by and interbedded with mudstone-dominated units that have a high organic carbon content. The unit below the Fusaru and Kliwa Sandstones is informally called the Lower 'Dysodilic' Shale and consists of thin-bedded very fine sandstone, siltstone and mudstone alternations.

The two studied exposures are located in two different thrust slices (Fig. 1b). Locality A is located in the Buzău Valley and exposes a thick-bedded sandstone unit underlain and overlain by finer grained, thin-bedded, mudstone-rich units (Figs 3 and 4a). The entire section belongs to the Fusaru Sandstone (Fig. 3). Locality B (Fig. 4b) exposes parts of the Lower Dysodilic Shale and contains a few muddy sandstone beds within a background of thin-bedded sandstone–mudstone couplets.

### Petrography

Fusaru Sandstone samples from locality A have a quartzofeldspathic composition with mean Q, F, L values of 65%, 28.5% and 6.5% respectively (Fig. 5). The average mica content is 6.5%. In contrast, framework grains in the mud-rich sands of locality B are dominated by monocrystalline quartz (97%). Glauconite is a minor but characteristic component of sandstone beds at locality B, whereas it occurs in the Fusaru Sandstone only in trace amounts. The interpreted source area for the Fusaru sands consisted mainly of plutonic

and medium-grade metamorphic rocks, with contributions from volcanic rocks, whereas the framework grains of muddy sands of locality B are polycyclic sediments. Palaeocurrents and palaeogeographic considerations suggest that the source area for the Fusaru Sandstone was situated towards the south (Fig. 2; Contescu *et al.*, 1967), possibly in the area corresponding to the present-day southern Carpathians. In contrast, the composition of sands from the Lower Dysodilic Shale might reflect an eastern, passive-margin source area, but there is no conclusive evidence from palaeocurrents at locality B.

The Fusaru Sandstone underwent rapid burial during the Oligocene and Miocene and associated cementation. Most of the mud-poor sandstones are well cemented; however, as the mud content increases, the rocks become less well cemented and therefore more friable.

The mud content of these sandstones is highly variable, from 2% to over 35%. Although minor amounts of weathered volcanic rock can be observed in the Fusaru Sandstone, most of the

Fig. 4. (a) Detailed measured section at locality A in the Fusaru Sandstone. Cross-bedded (cb), finer grained mud-rich (fm), coarser grained mud-rich (cm) units and sampled intervals (arrows) are shown on the right side of the column. Event bed labels (TB and SB) refer to whether the beds contain one or more mud-rich divisions (slurry beds, SB) or not (turbidites, TB). (b) Measured section of locality B belonging to Lower 'Dysodilic' Shale, consisting of fine-grained turbidites with thick muddy caps and four slurry beds. Sampled beds are marked with arrows in both sections. Note different scales.



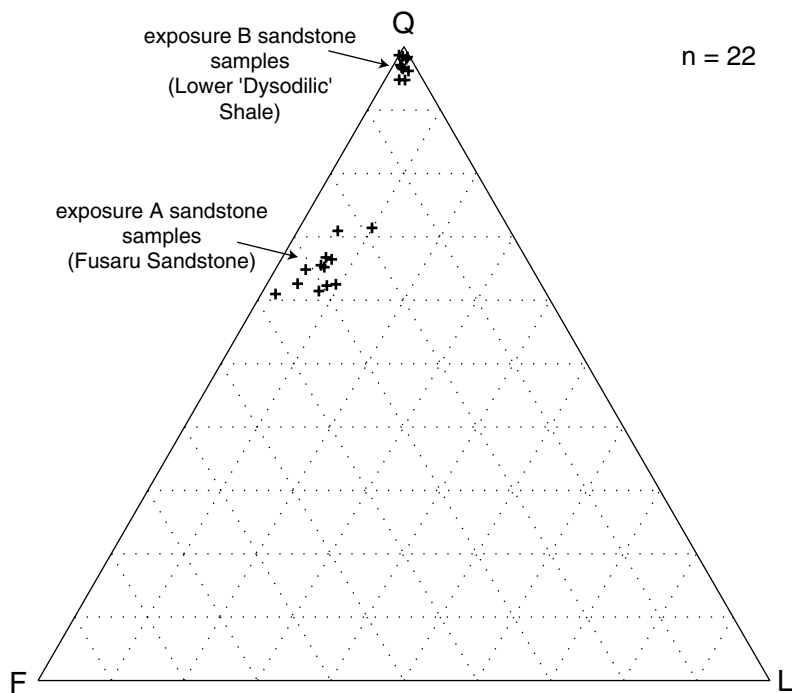


Fig. 5. QFL ternary plot of 22 sandstone samples from outcrops A and B, based on point counting.

mud is detrital. Volcanic rock fragments tend to preserve their original textures and shapes and can thus be distinguished from mud floccules, small mud chips and the muddy matrix. The last is finely granular, dark coloured and pore filling. In addition to petrographic criteria, several other observations support the detrital, non-diagenetic origin of the mud. First, mud-rich and mud-poor sandstones are intimately interbedded at scales ranging from laminae to beds. The hydrodynamic behaviour of alterable clastic rock fragments is not different enough from that of quartz and feldspar to result in such a strong segregation. The interbedded mud-rich and mud-poor layers do not seem to have different source areas; the framework grains of the mud-rich and mud-poor samples of the Fusaru Sandstone all have similar compositions. Secondly, fluid escape channels in mud-rich beds usually contain much less mud than the surrounding sediment. This probably reflects elutriation of fine mud particles along these flow paths during fluid escape, indicating that mud was present as hydraulically fine particles at the time of deposition and dewatering.

## DEPOSITIONAL SETTING

The sand-rich section at locality A sharply overlies a thin-bedded mudstone-dominated sequence. The thickest and coarsest beds appear

to occur towards the base of the sandy section (Fig. 4a), although Kendall's rank correlation test (Harper, 1998; Chen & Hiscott, 1999) indicates that only the upward-fining trend is significant at the 5% level. The same sandstone interval is exposed about 1.5 km to the SW of locality A, where its lower bounding surface can be traced over a distance of about 400 m. This surface downcuts at least 20 m across bedding into the underlying thin-bedded section. At this locality, the sandstones fill and onlap the sides of an erosional depression. This architecture and facies organization resembles many upward-fining units interpreted as abandoned or backfilled channels (e.g. Chen & Hiscott, 1999).

Locality B exposes fine-grained, thin-bedded turbidites, with only a few mud-rich sandstone beds. The lack of thick-bedded facies and of significant erosion or amalgamation suggests that this exposure represents unchanneled sheet deposits.

## EVENT-BED TYPES

### Mud-poor, thick sandstone beds

#### Observations

About 85% of the beds measured at locality A are thicker than 0.3 m, and most consist of mud-poor sandstone. The studied sandstones have a

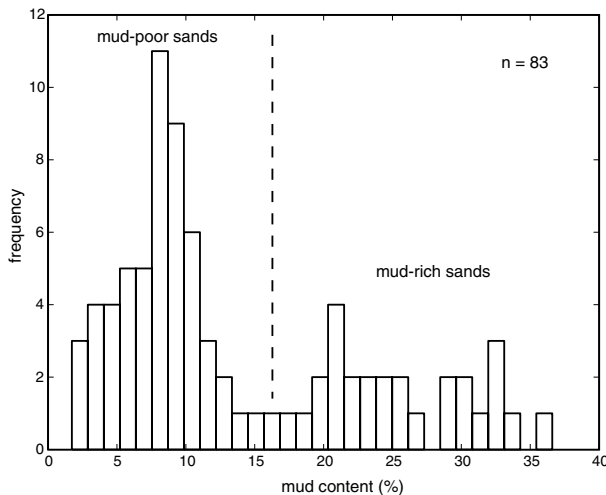


**Fig. 6.** Volumetric mud content values of 83 samples from the Fusaru Sandstone and the Lower 'Dysodilic' Shale, localities A and B.

bimodal distribution in terms of mud content (Fig. 6): samples either contain about 3–13% or more than 20% detrital mud. The first group will be referred to as mud-poor sandstones; the second group will be referred to as mud-rich sandstones.

The maximum thickness of the mud-poor sandstone beds is 5.8 m, but the median bed thickness at locality A is 85 cm. The particles range from very fine sand to pebbles up to 7 mm in diameter. However, most beds consist of massive, poorly sorted (Fig. 7b) sandstone with a mean grain size of 2.5  $\phi$  to 3.25  $\phi$  (100–175  $\mu\text{m}$ ; Fig. 7a) corresponding to fine to very fine sand. Only cross-laminated divisions in the upper parts of beds have finer average grain sizes (3.25–4.3  $\phi$  or 50–100  $\mu\text{m}$ ; Fig. 7a). The lower, massive parts of thicker beds usually have a small population of granules and pebbles that make the sediment bimodal. However, this coarse component is not captured by the textural analyses based on thin sections. If studied only in the outcrop, such beds are described as normally graded because the granules and pebbles are easy to observe and typically occur only towards the bases of beds.

The mud-poor sandstone beds of locality A can be described in terms of the turbidite divisions of Bouma (1962) and Lowe (1982). Most have a well-defined, sharp base overlain by bimodal sand containing dispersed granules (Fig. 4a) and lacking traction structures. The granules and pebbles fine and gradually disappear upwards in the beds, resulting in coarse-tail normal grading. These sediments lack traction structures and correspond to the  $S_3$  division of Lowe (1982). Dish structures are common and tend to occur towards the bases

of the thickest beds (Fig. 4a). Water-escape channels that are often sheared and inclined are present towards the tops of  $S_3$  divisions in some beds (Fig. 8a). The  $S_3$  divisions are usually overlain by Bouma  $T_{bcd}$  divisions that are better developed in the upper part of the studied section, where many  $T_c$  divisions are very fine grained (Fig. 7a) and associated with mud-rich sandstone (Figs 4 and 8b–d; see below). Climbing ripple cross-lamination is common in the thicker  $T_c$  divisions.

Large-scale (dm) cross-stratification occurs in four places at locality A. Although definition of individual event beds is more difficult when cross-stratification is present, three cross-bedded divisions appear to occur at the tops of  $S_3$  units (Fig. 4a). These cross-bedded sandstones are coarser and better sorted than the underlying  $S_3$  divisions. Comparably coarse and well-sorted lenses of coarse sandstone can also occur within the middle or upper parts of  $S_3$  divisions.

#### Interpretation

The mud-poor, thick-bedded sandstones at locality A are interpreted as the deposits of high-density turbidity currents. Plane-lamination, cross-lamination and cross-bedding can form only during transport and deposition from turbulent flows (Middleton & Southard, 1984). The lack of traction structures in thick  $T_a/S_3$  units is probably due to suspended-load fallout rates sufficiently high to suppress bedload development and traction transport (Lowe, 1982; Arnott & Hand, 1989; Allen, 1991).

#### Event beds with mud-rich divisions

##### Observations

Several layers in the upper part of the section at locality A (Fig. 4a) and four beds in outcrop B (Fig. 4b) have a distinctly dark colour, are weakly lithified and have higher mud contents than the mud-poor sandstones described above. They range from 10 to 50 cm in thickness and show mud contents from 15% to over 35% (Figs 6 and 7). These mud-rich sandstones can be divided into two groups: (i) poorly sorted, coarser mud-rich sandstones with a mean grain size of about 3  $\phi$  (fine to very fine sand); and (ii) well-sorted finer sandstones with an average grain size of slightly more than 4  $\phi$  (very fine sand to coarse silt; Fig. 7). There is no transition between these two groups: samples with intermediate grain sizes correspond mainly to  $T_b$  divisions and have low mud contents (Fig. 7a).

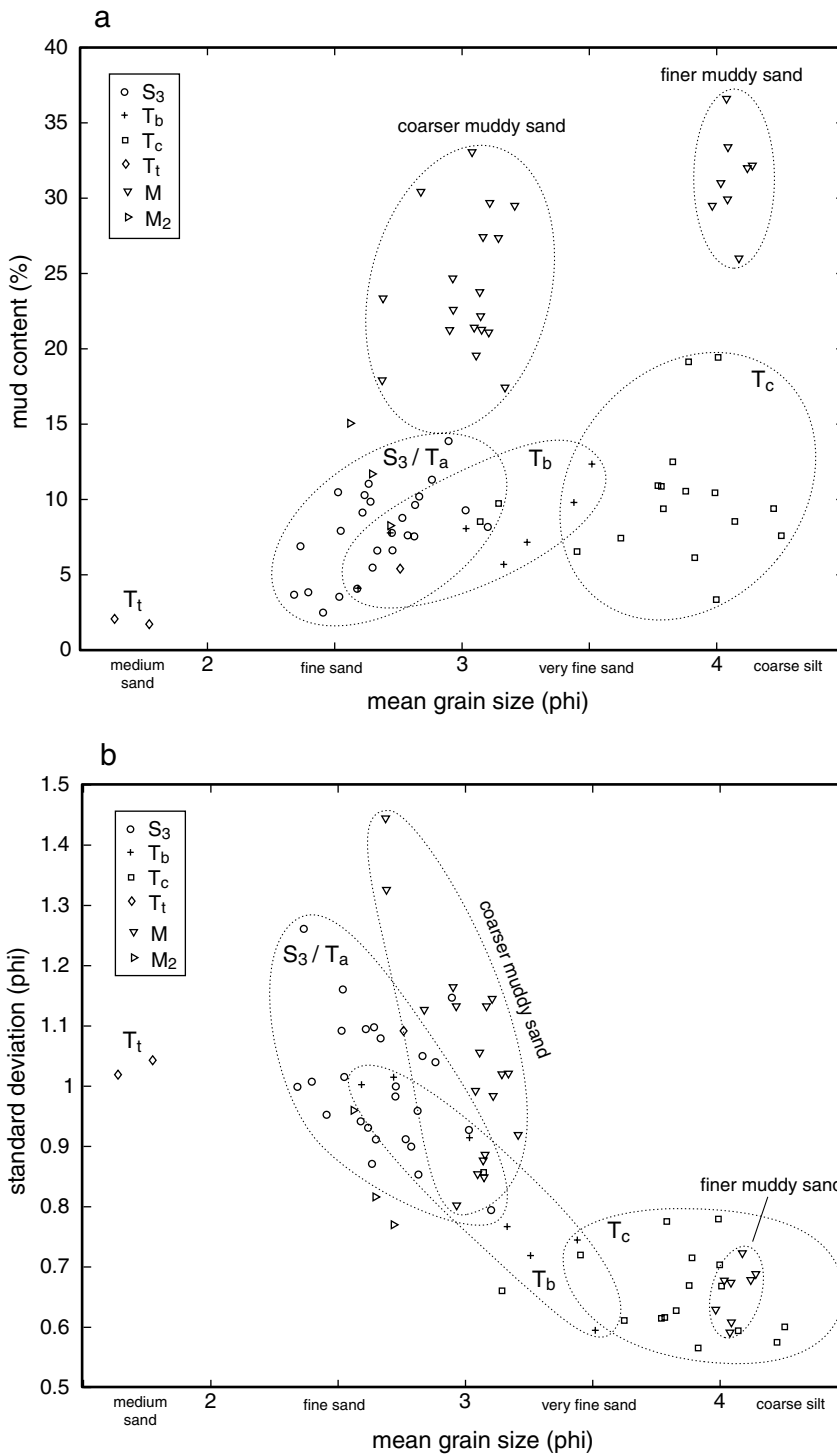


**Fig. 7.** Mud content (a) and sorting represented by the standard deviation (b) of sandstone samples, as a function of their mean grain size. Samples are grouped according to the turbidite/slurry bed divisions they come from. M is mud-rich sand, M<sub>2</sub> is the mesobanded division of Lowe & Guy (2000).

Sandstones of the former, coarser group are slightly finer grained and, for the same mean grain size, are less well sorted than samples from S<sub>3</sub> divisions (Figs 7 and 9). Most lack traction structures, although diffuse parallel lamination is present in some beds. Meso- to microbanding (Lowe & Guy, 2000) occurs in mud-rich sands at

locality B (Figs 10 and 11), although it is not as well developed as similar banding described by Lowe & Guy (2000). Slabbed samples from the lower part of bed SB5 (Fig. 4) show alternating dark and light bands with soft-sediment deformation and water-escape structures (Fig. 11). The thicker light bands have commonly foundered

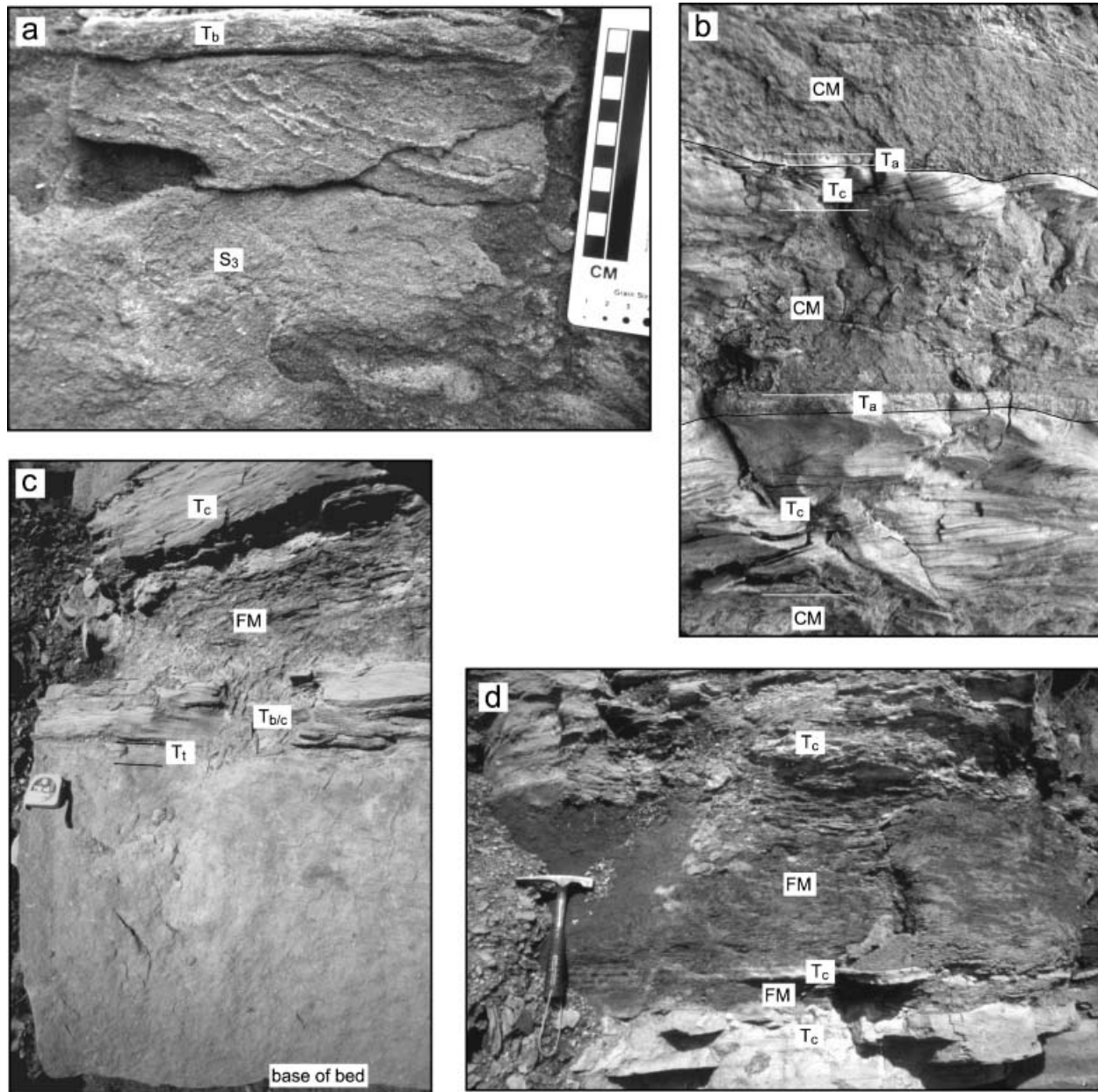


**Fig. 8.** Photographs of event beds at locality A. Bouma divisions, coarser grained muddy sand (CM) and finer grained muddy sand (FM) units are marked. (a) Sheared water-escape sheets at the top of an  $S_3$  division in sampled interval SB3. Mud content is about 10%. (b) Two  $T_c$  units of very fine-grained sandstone, belonging to two separate event beds, overlain with a sharp grain-size break by two coarser grained muddy divisions. Bed boundaries are shown by black lines. Note thin, light, mud-poor layers (marked as  $T_a$ ) at the base of the muddy sandstone. Interval shown is 24 cm thick. (c) Sampled interval SB2, with locally developed lenses of coarse sandstone at the top of the  $S_3$  unit ( $T_t$  division) and a thick unit of very fine-grained muddy sandstone (FM). (d) Upper part of sampled interval SB1, with alternating units of ripple-laminated very fine-grained sandstone and muddy sandstone of a similar mean grain size. Note the weakly developed horizontal lamination in the muddy units (FM), especially where they are transitional towards  $T_c$  divisions.

into the underlying muddy dark layers and are cut by sets of subparallel light-coloured water-escape sheets lacking mud (Fig. 11). The upper parts of the mud-rich beds at locality B commonly contain mudclasts (Fig. 10a) and light-coloured

sand masses and lobes that formed through foundering of relatively mud-poor sediment into underlying muddier layers (Fig. 10b).

The finer grained mud-rich sandstones have mean grain sizes and sorting that are essentially

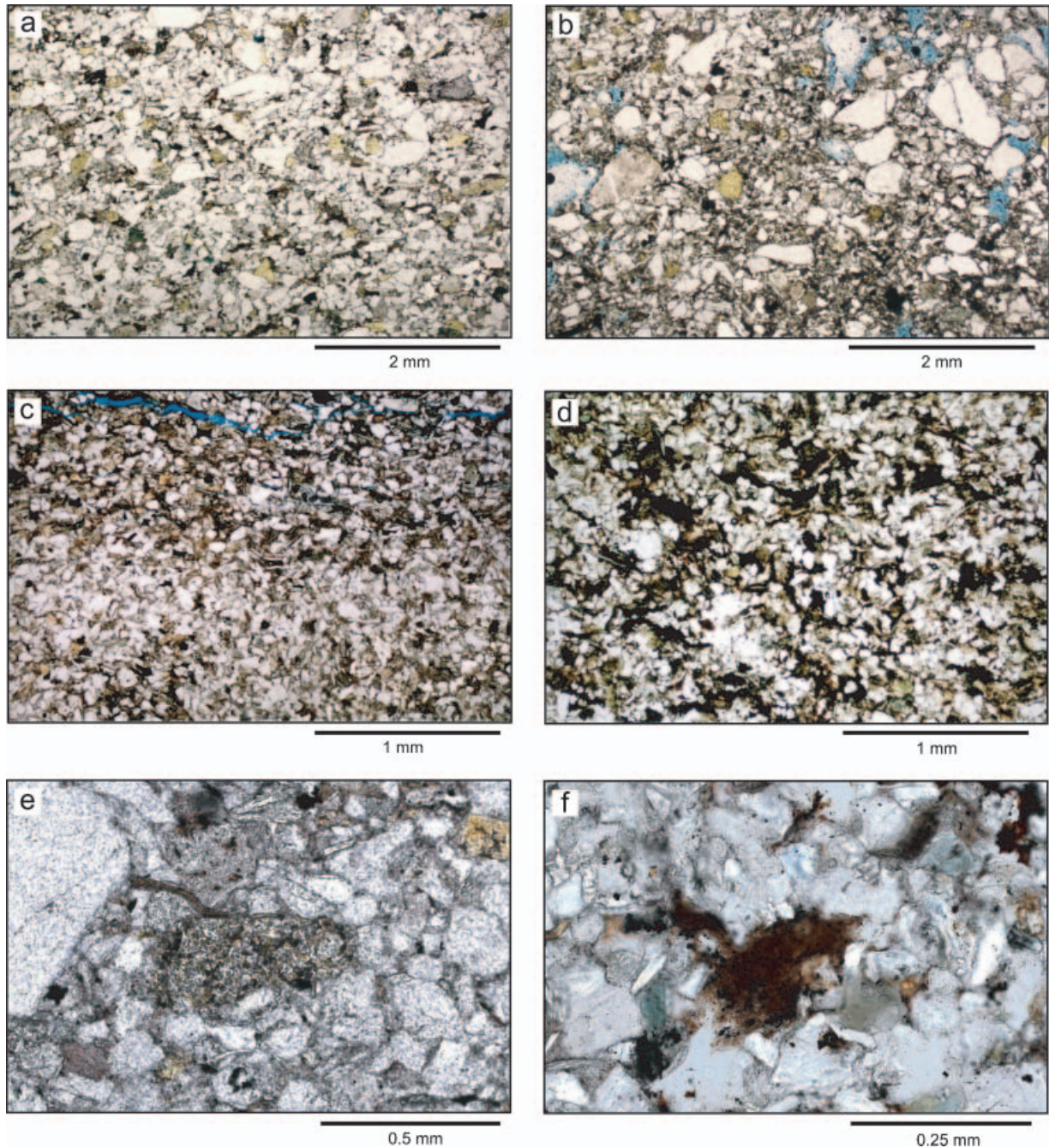


**Fig. 9.** Photomicrographs of coarser (a and b) and finer (c and d) sandstones. Thin sections were stained for K-feldspar. (a) Mud-poor sandstone from an  $S_3$  division (sample TB3-a, Fig. 4), in plain light, with mean grain size  $2.72 \phi$  ( $0.152 \text{ mm}$ ) and sorting  $0.98 \phi$ . Note the relatively well-developed grain orientation. (b) Mud-rich sandstone (sample SB3-p), with mean grain size  $2.69 \phi$  ( $0.155 \text{ mm}$ ) and sorting  $1.33 \phi$ . Although the mean grain size is similar to that in (a), the standard deviation is much larger. This sediment has no well-developed grain orientation. (c) Mud-poor, very fine sandstone (mud-poor part of sample SB1-m). The lower part is slightly coarser and contains less mica and mud than the upper part. (d) Mud-rich, very fine sandstone or siltstone (sample SB1-l), with a mud content of 36.6%, mean grain size  $4.04 \phi$  ( $0.061 \text{ mm}$ ) and sorting  $0.59 \phi$ . Some of the dark particles consist of clay rich in organic matter. Note poor grain orientation compared with the mud-poor sand in (a). (e) Example of a volcanic rock fragment in thin section. Compare it with (f) a typical muddy particle.

indistinguishable from those of  $T_c$  divisions (Fig. 7). Diffuse parallel lamination is better developed in these units than in the coarser beds

(Fig. 8c and d). This lamination seems to be transitional between microbanding and parallel lamination of  $T_{de}$  divisions in fine-grained turbidites

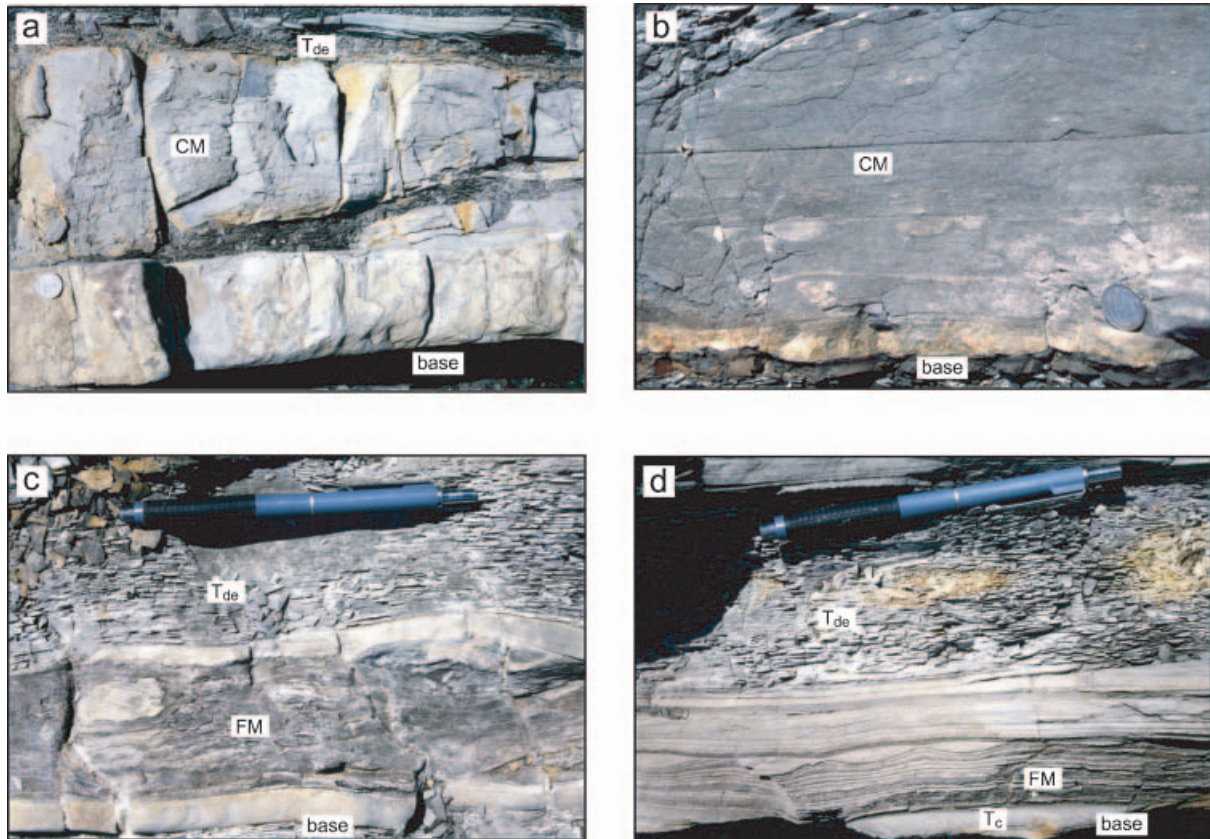


**Fig. 10.** Photographs of event beds at locality B. Lettering as in Figs 1b and 4. The beds shown in (a) to (d) represent a spectrum of deposits from the coarsest (a) to the finest (d). (a) Sampled bed SB5 has a lower, less muddy unit that consists of a dark and a light band (Fig. 11), and an upper, muddier unit with mud clasts. Coin for scale has a diameter of 2 cm. (b) Coarser grained muddy sand bed with three light bands in its lower part. Note load structures under the third light band. Coin for scale has a diameter of 2 cm. (c) An event bed with two light bands and a finer muddy sand division, overlain by a thick laminated  $T_{de}$  division that consists of silt and mud. (d) A sedimentation unit with a very fine-grained sandy  $T_c$  division at the base overlain by microbanded finer grained muddy sand and silt (FM). This unit is transitional toward the parallel lamination of a 'normal' fine-grained turbidite.

(Fig. 10d; Piper, 1978; Stow & Bowen, 1980). In thin section, small-scale variability in mud content of the sands is evident (Fig. 9c). Thin mud-rich laminae may comprise more than 50–60% mud. The increased mud content is associated with an increase in the percentage of mica and organic fragments and a deterioration in the parallel grain fabric (Fig. 9). When present, the mudclasts are typically larger than the sand grains (Fig. 9d).

#### Interpretation

These mud-rich sands show features suggesting deposition by flows similar to the slurry flows described by Lowe & Guy (2000), which exhibit both turbulence and cohesive behaviour. The common presence of a weakly developed parallel lamination (Figs 8c and d and 10c) and of meso- and microbanding (Figs 10 and 11) suggest

grain-size segregation resulting from traction movement and deposition beneath turbulent flows. Individual dark mud-rich layers and bands that lack lamination and show a chaotic fabric in thin section (Fig. 9d) represent thin mud-rich shear layers or cohesive debris flows at the bases of turbidity currents. Lowe & Guy (2000) suggested that banding forms beneath mud-rich turbidity currents as flow stratification becomes more pronounced and the lower, denser part of the flow is progressively enriched in mud relative to quartz and feldspar. This occurs because, although both sand-sized mud and quartz grains settle out of suspension, denser quartz and feldspar grains settle to the bed preferentially and are deposited as part of a light band. The gradual increase in mud content of the basal part of the flow results in the formation of a cohesive near-bed shear layer that eventually freezes as a

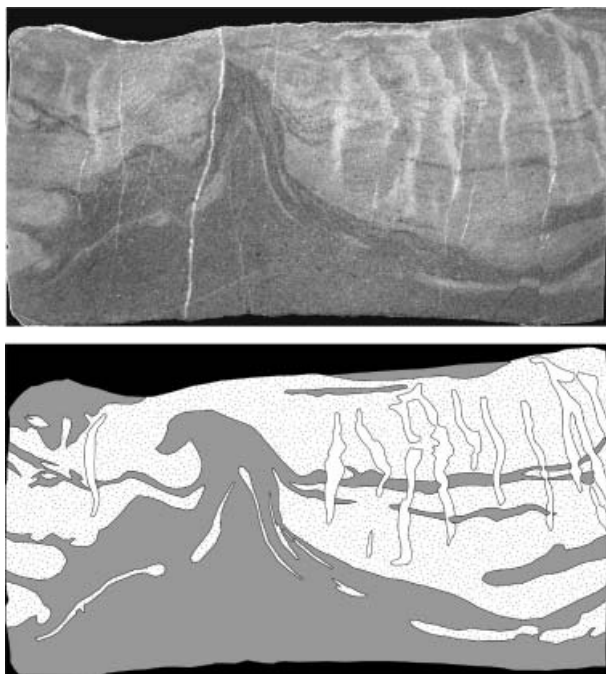


**Fig. 11.** A couplet of dark and light bands in the lower part of slurry bed SB5 (Fig. 10a), showing subsidence lobes with water-escape sheets. The differences in mud content are low, but the light band is slightly less muddy than the dark band and the water-escape conduits are mud free. Thickness of the couplet is 10 cm.

dark band. When the strength of the mud-rich layer is high enough that quartz and feldspar grains cannot settle through it, they begin to accumulate on the top of the dark layer, forming the lower part of a new light band (Lowe & Guy, 2000). The horizontal banding and/or lamination of the mud-rich divisions described here probably have broadly similar origins. Baas & Best (2002) have shown experimentally how Kelvin–Helmholtz instabilities along the basal shear layer of transitional flows can result in periodic lamina formation. On a larger scale, such instabilities could contribute to the formation of the banding observed in many slurry beds.

## TEXTURAL TRENDS

Figure 12 illustrates the textural trends in three mud-poor sandstone beds interpreted as turbidites, TB1, TB2 and TB3 from locality A (Fig. 4a). Turbidite TB1 is 3 m thick and dominated by a thick  $S_3$  division with granules and dish structures at its base. TB2 is 120 cm thick and has a coarse-grained lens at the transition between the  $S_3$  and  $T_b$  divisions. TB3 is 60 cm thick and has

well developed  $T_a$ ,  $T_b$  and  $T_c$  divisions. Four other beds, SB1, SB2, SB3 and SB4 (Figs 13 and 14), are characterized by the presence of mud-rich sandy divisions within sequences of sedimentary structures that resemble the Bouma turbidite divisions.

The textural trends within these units are not substantially different from those in the normal turbidites. Figure 15 and Table 1 summarize the statistically significant vertical grain-size trends in the  $S_3/T_a$ ,  $T_{bcd}$  and muddy divisions. These summaries suggest that (1) inverse grading and especially inverse fine-tail grading are common in  $S_3/T_a$  divisions and not present in  $T_{bcde}$  or muddy divisions, which are more likely to be normally graded; (2) grading trends are strongest in  $T_{bcde}$  units and less well developed in  $S_3/T_a$  divisions; and (3) upward improvement in sorting characterizes most beds of all types. Normal grading is common, especially in the form of distribution grading of Bouma  $T_{bcde}$  divisions. Normal grading of the  $S_3/T_a$  division is weakly developed and only detectable in the coarsest sizes, which tend to be under-represented in thin sections.

Several quantitative textural studies of turbidites have shown that, even where the mean grain size lacks normal grading (Middleton, 1962) or where inverse-to-normal grading is present (Middleton, 1967), sorting improves upwards within beds. The turbidites of the Fusaru Sandstone show the same pattern: both normally and inversely graded intervals tend to show an upward improvement in sorting (Figs 12–14). In contrast, ungraded intervals tend to be relatively poorly sorted and lack significant upward changes in sorting.

Sampled intervals that lack grading in mean grain size (SB3, SB4, SB5; Figs 13 and 14) tend to have higher mud contents than ones with clearer trends. However, the lack of grading in the mean can be accompanied by poorly developed inverse fine-tail grading and normal coarse-tail grading.

The uppermost sample from TB1 is from a flat-laminated  $T_b$  division (Fig. 12). This division is overlain by a 10 cm thick unit of cross-stratified sandstone that is capped by very fine-grained  $T_d$  and  $T_e$  divisions. It is evident in outcrop that the relatively thick  $T_{de}$  divisions at the top are normally graded. Thus, in terms of mean grain size, the whole bed shows overall inverse-to-normal grading (Fig. 12). The sample from the laminated  $T_b$  division (Fig. 12) is apparently more poorly sorted than the underlying sample

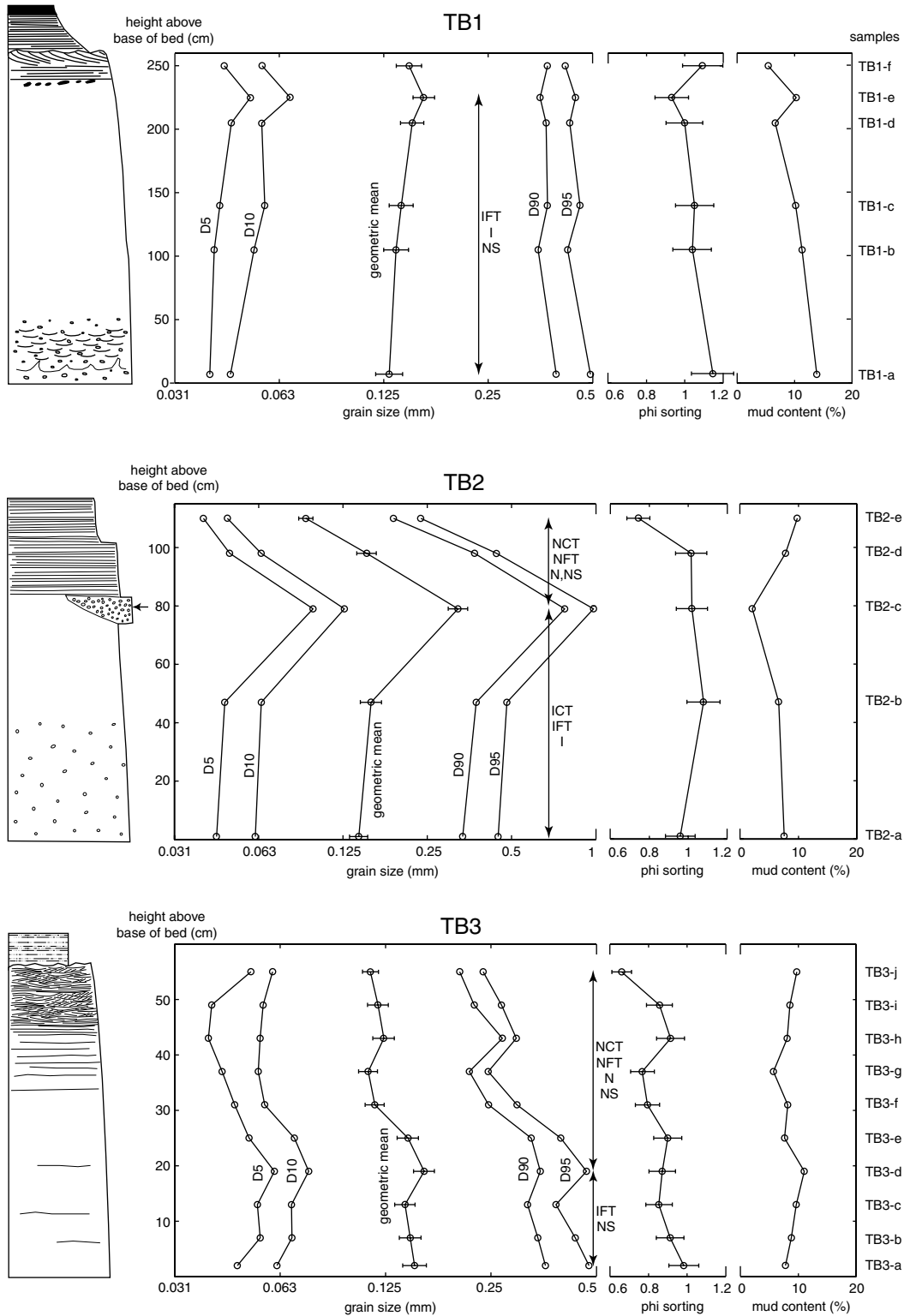


**Fig. 12.** Grain-size trends in beds TB1, TB2 and TB3 (for location, see Fig. 4a). Error bars on mean grain size and standard deviation represent a 95% confidence interval. The mean grain size was calculated on data in  $\phi$  format; therefore, it represents a geometric mean. Arrow on the sedimentological column shows exact location of sample where its position is ambiguous. Arrows on the data plots mark the intervals that were tested for vertical grain-size trends. Key is the same as in Fig. 4. NCT, normal coarse-tail grading; NFT, normal fine-tail grading; N, normal grading (based on the geometric mean); ICT, inverse coarse-tail grading; IFT, inverse fine-tail grading; I, inverse grading (based on the geometric mean); NS, upward improvement of sorting; IS, upward deterioration of sorting.

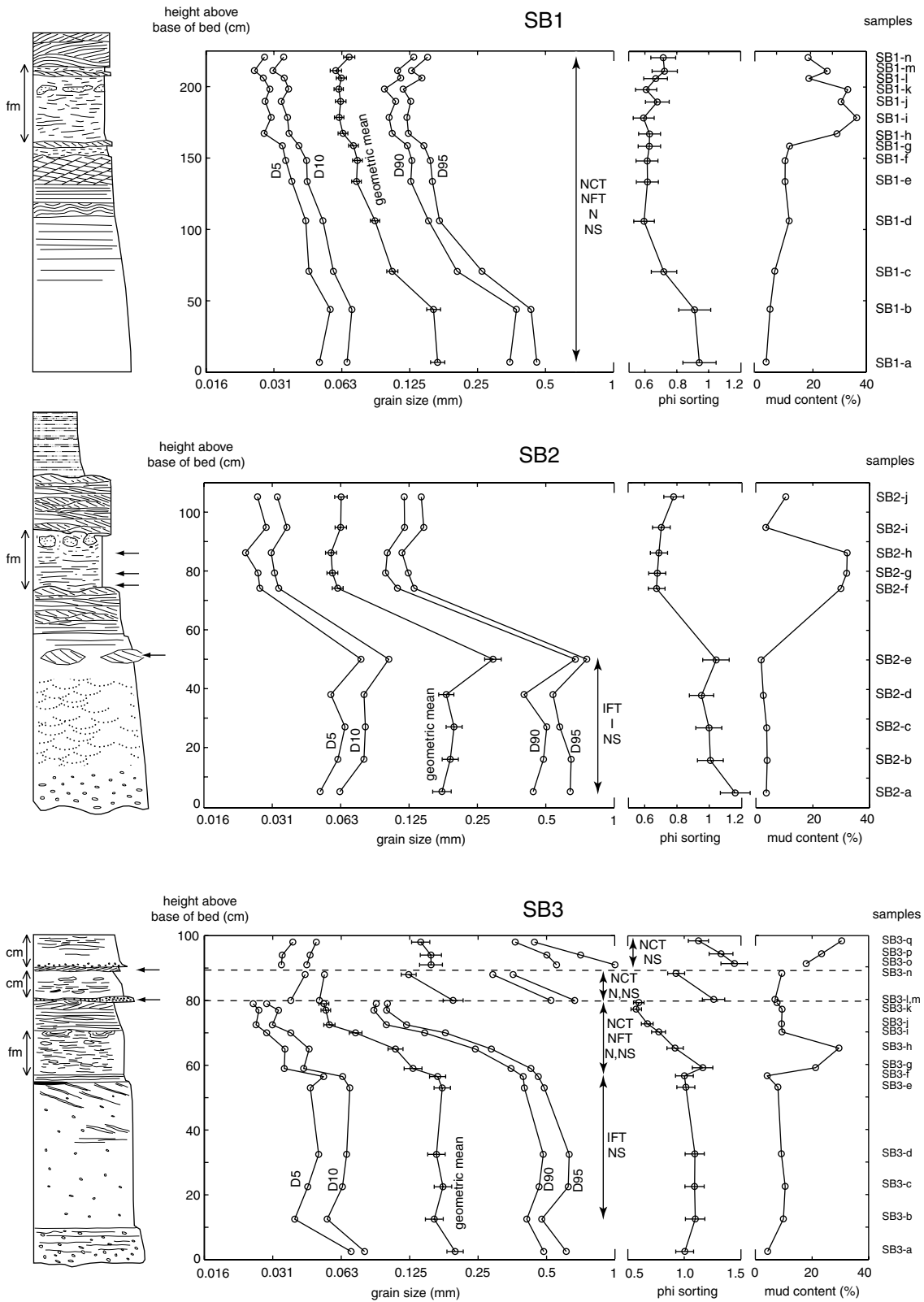


Fig. 13. Grain-size trends in beds SB1, SB2 and SB3 (for location, see Fig. 4a). For explanations, see caption to Fig. 12.

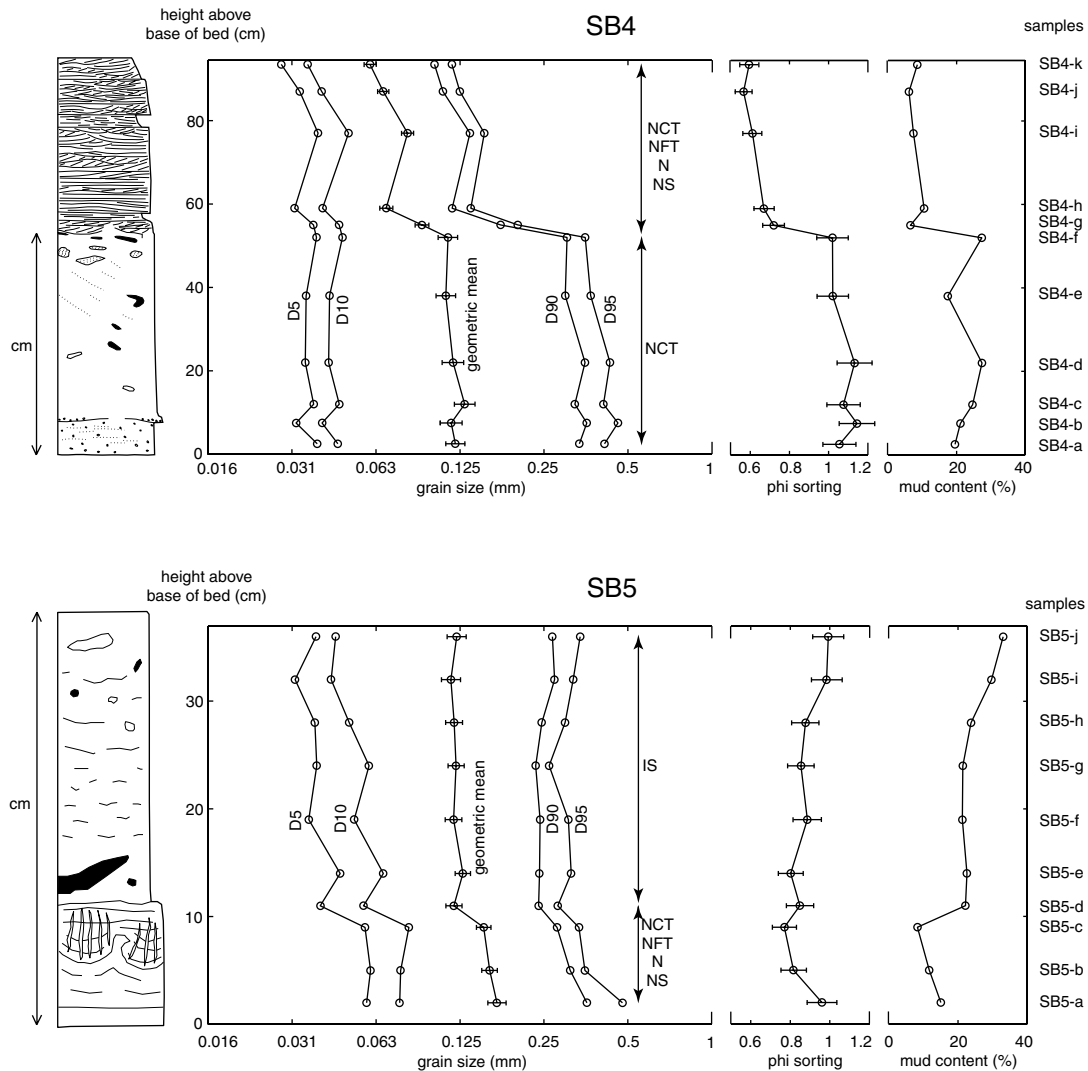


Fig. 14. Grain-size trends in beds SB4 and SB5 (for location, see Fig. 4a). For explanations, see caption to Fig. 12.

from the massive division. This, however, is the result of counting both coarser grained and finer grained laminae together. In fact, the individual thin layers that compose the  $T_b$  division are well sorted. Such well-structured, laminated divisions with well-sorted layers of light colour overlie the  $S_3$  division in several other beds in the Buzău Valley section (Fig. 4a). They are coarser grained than the 'standard'  $T_b$  division and occur at the tops of thick  $S_3$  units. Some of the cross-bedded units of the Fusaru Sandstone might belong to the same category. In TB2 (Fig. 12) and SB2 (Fig. 13), lenses of medium-grained sand are present at the transition from  $S_3$  to  $T_b$ , with sediment coarser than the under- and overlying deposits. However, the maximum grain size does not exceed the size of the largest grains in the underlying  $S_3$  division.

## INTERPRETATION OF VERTICAL GRAIN-SIZE TRENDS

### Thick inversely graded divisions in mud-poor sandstones

In addition to the examples described here, textural studies of thick-bedded deep-water sandstones lacking traction structures and experiments on sedimentation from high-concentration and high-velocity flows (see References in Table 2) suggest that grading types other than normal are relatively common in such deposits. The outcrop examples of Gonzalez-Bonorino & Middleton (1976) include basal inversely graded zones (Table 2) that could not have been deposited by single traction carpets because they are thicker than the maximum sediment weight that

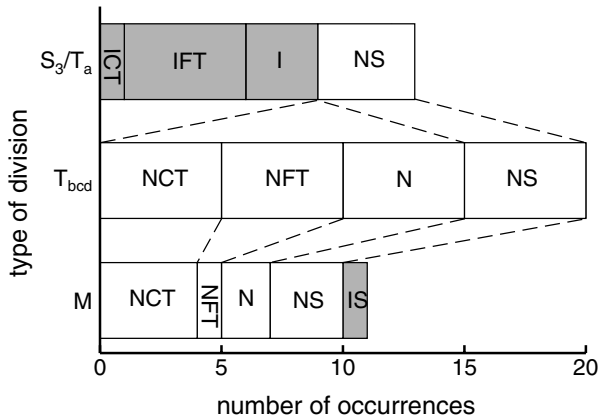


**Fig. 15.** Number of statistically significant different vertical grain-size trends as a function of sedimentary division type. NCT, normal coarse-tail grading; NFT, normal fine-tail grading; N, normal grading (based on the geometric mean); ICT, inverse coarse-tail grading; IFT, inverse fine-tail grading; I, inverse grading (based on the geometric mean); NS, upward improvement of sorting; IS, upward deterioration of sorting.

can be supported by dispersive pressure for the given grain size (Lowe, 1976). No traction carpets with well-developed dispersive pressure and inverse grading were observed in the experiments of Vrolijk & Southard (1997). The 240 cm thick inversely graded  $S_3$  division of TB1 (Fig. 12) is far too thick to have formed as a single traction carpet supported by dispersive pressure (Lowe, 1976). The weak normal grading of the largest particles within this bed is also inconsistent with its having formed through traction carpet sedimentation, inasmuch as large grains are more strongly affected by dispersive pressure and should show the most pronounced inverse grading. Furthermore, experimental work suggests that increasing shear rates actually prevent the development of inverse grading (Legros, 2002).

Apart from suggestions for winnowing as the cause of inverse grading (Banerjee, 1977; Kranck, 1984), other interpretations link the increase in grain size to changes in mean current velocity. Perhaps the dominant view (Kneller, 1995; Kneller & Branney, 1995; Mulder & Alexander, 2001) is that thick inversely graded layers form under waxing flow conditions, and mud-poor ungraded intervals reflect deposition from sustained, quasi-steady flows that possibly originate as hyperpycnal flows. Thus, it has been suggested that inverse grading at the base of a turbidite could be a diagnostic feature of waxing quasi-steady hyperpycnal flow deposits. However, the inverse grading at the base of many experimental deposits of Vrolijk & Southard (1997) formed beneath rapidly

decelerating and depositing flows, not under conditions characteristic of quasi-steady hyperpycnal currents. Sedimentation rates of up to  $2 \text{ cm s}^{-1}$  were observed in these experiments. Such sedimentation rates combined with long-lived, sustained currents would result in structureless sands of enormous thicknesses, which have not been observed in the geological record.

Interpretations that link grain-size variations to changes in flow velocity fail to consider that most depositing turbidity currents are overloaded, suspended-load fallout rates are high, and it is capacity, not competence, that drives sedimentation (Kuenen & Sengupta, 1970; Lowe, 1988; Allen, 1991; Hiscott, 1994a). The effects of overloading and high suspended-load fallout rates must be even stronger in the case of the Bouma  $T_a$  or Lowe  $S_3$  divisions than during deposition of the current-structured units. In addition, the numerical modelling of Felix (2002) shows that velocity influences the distribution of grains in the flow only through the production of turbulence. Thus, the vertical changes in mean grain size of thick-bedded deep-water sands lacking traction structures might differ substantially from the flow hydrograph of the depositing current at the same location.

An alternative and simpler explanation for the textural trends described above takes into account that changing flow concentration and the associated sediment deposition rate can result in variable degrees of entrapment of fines in the deposit. Sediment deposition from sand-rich turbidity currents tends to be rapid (Lowe, 1982), with a sedimentation rate that almost instantaneously reaches a maximum and then decreases with time (Allen, 1991; Middleton, 1993). In the case of turbidite TB1 (Fig. 12), as deposition begins, suspended-load fallout rates are highest. Under conditions that are comparable to the experiments of Vrolijk & Southard (1997), deposition rates are high enough so that neither traction nor traction carpets develop. Deposition is driven by capacity, and a significant amount of fine-grained sediment, including up to 14% mud, is trapped in the deposit. As the rate of deposition declines, the amount of trapped fines is gradually reduced. This change becomes clear in the anticlockwise rotation of cumulative probability plots in Fig. 16a and in the progressive transformation of the curves of normal distribution that were fitted to the original grain-size distributions from the  $S_3$  division of TB1 (Fig. 17a). The loss of fine material upwards within the bed can be explained as a trapping effect that decreases as the

**Table 1.** Results of statistical analysis of vertical grain-size trends in 15 intervals in event beds of the Fusaru Sandstone and Lower 'Dysodilic' Shale.

Bed	Interval	Division	No. of samples	P-value of coarse-tail trend	P-value of fine-tail trend	P-value of median trend	P-value of sorting trend	NCT	ICT	NFT	IFT	N	I	NS	IS
TB1	TB1a-TB1e	T <sub>a</sub>	5	0.139	<b>0.001</b>	< <b>0.001</b>	< <b>0.001</b>	No	No	No	Yes	No	Yes	Yes	No
TB2	TB2a-TB2c	T <sub>a</sub>	3	< <b>0.001</b>	< <b>0.001</b>	< <b>0.001</b>	0.193	No	Yes	No	Yes	No	Yes	No	No
TB2	TB2c-TB2e	T <sub>bd</sub>	3	< <b>0.001</b>	< <b>0.001</b>	< <b>0.001</b>	< <b>0.001</b>	Yes	No	Yes	No	Yes	No	Yes	No
TB3	TB3a-TB3d	T <sub>a</sub>	4	0.351	<b>0.045</b>	0.082	<b>0.016</b>	No	No	No	Yes	No	No	Yes	No
TB3	TB3d-TB3j	T <sub>bd</sub>	7	< <b>0.001</b>	<b>0.02</b>	< <b>0.001</b>	<b>0.004</b>	Yes	No	Yes	No	Yes	No	Yes	No
SB1	SB1a-SB1n	T <sub>ad</sub>	14	< <b>0.001</b>	< <b>0.001</b>	< <b>0.001</b>	< <b>0.001</b>	Yes	No	Yes	No	Yes	No	Yes	No
SB2	SB2a-SB2e	T <sub>a</sub>	5	0.263	<b>0.001</b>	< <b>0.001</b>	<b>0.018</b>	No	No	No	Yes	No	Yes	Yes	No
SB3	SB3b-SB3f	T <sub>a</sub>	5	0.144	<b>0.02</b>	0.254	<b>0.023</b>	No	No	No	Yes	No	No	Yes	No
SB3	SB3f-SB3l	T <sub>bd</sub>	7	< <b>0.001</b>	< <b>0.001</b>	< <b>0.001</b>	< <b>0.001</b>	Yes	No	Yes	No	Yes	No	Yes	No
SB3	SB3m-SB3n	M	2	< <b>0.001</b>	0.113	< <b>0.001</b>	< <b>0.001</b>	Yes	No	No	No	Yes	No	Yes	No
SB3	SB3o-SB3q	M	3	< <b>0.001</b>	0.191	0.493	< <b>0.001</b>	Yes	No	No	No	No	No	Yes	No
SB4	SB4a-SB4f	M	6	<b>0.007</b>	0.414	0.149	0.062	Yes	No						
SB4	SB4f-SB4k	T <sub>cd</sub>	6	< <b>0.001</b>	< <b>0.001</b>	< <b>0.001</b>	< <b>0.001</b>	Yes	No	Yes	No	Yes	No	Yes	No
SB5	SB5a-SB5d	M	4	< <b>0.001</b>	<b>0.004</b>	< <b>0.001</b>	<b>0.025</b>	Yes	No	Yes	No	Yes	No	Yes	No
SB5	SB5d-SB5j	M	7	0.061	0.111	0.406	< <b>0.001</b>	No	Yes						

NCT, normal coarse-tail grading; ICT, inverse coarse-tail grading; NFT, normal fine-tail grading; IFT, inverse fine-tail grading; N, normal grading in the mean; I, inverse grading in the mean; NS, upward improvement in sorting; IS, upward decrease of sorting. *P*-values smaller than 0.05 are highlighted in bold.

**Table 2.** Examples of inverse grading in sediment gravity-flow deposits that probably did not develop through dispersive pressure.

	Deposits	No. of beds with probable inverse grading	Thickness of beds	Notes
Middleton (1962)	Normanskill Fm., New York	2 out of 6	230 and 366 cm	Both beds show NCT and IFT grading
Gonzalez-Bonorino & Middleton (1976)	Punta Negra Fm., Argentina	4 out of 9	102, 60, 30, 240 cm	The thickest bed is inversely graded; the rest show inverse-to-normal grading
Hiscott & Middleton (1979)	Tourelle Fm., Quebec	1 out of 3	?	Part of bed 6a shows NCT and IFT grading
Hiscott & Middleton (1980)	Tourelle Fm., Quebec	3 out of 10	1050, 230, 1500 cm	Inverse-to-normal grading
Migeon <i>et al.</i> (2001)	Sediment waves on the Var Sedimentary Ridge (SE France)	One clear example (sequence V)	40 cm	Inverse-to-normal grading; fine sediment content decreases upward
Middleton (1967)	Experimental turbidity current deposits		≈ 1 cm	Normal grading only shown by coarse tail; inverse-to-normal grading
Vrolijk & Southard (1997)	Experimental deposits of decelerating suspension currents	7 out of 11	18–39 cm	Most deposits are inverse-to-normally graded

NCT, normal coarse tail; IFT, inverse fine tail.

rate of deposition declines. In the case of TB1, the entrapment rate decreases strongly enough to result in inverse grading of the average grain size (Figs 12 and 17a). The coarse tail of the distribution stays essentially fixed throughout this change: no grains coarser than the coarse tail of the basal sample were deposited. In fact, in terms of maximum grain size, TB1 is weakly normally graded. This is suggested by the presence of granule-grade material only in the lower part of the bed (not captured by the thin sections). The progressive removal of fines results in the following upward changes in the shape of the normal fit curves (Fig. 17a): (1) an increasing mean grain size; (2) a reduction in dispersion that corresponds to an improvement in sorting; (3) a well-developed inverse fine-tail grading; (4) an increasing positive skewness (long fine tail due to incompleteness of removal of fines); and (5) an increasing kurtosis, that is the curves become more leptokurtic. The gradually decreasing mud content of the sand also reinforces the interpretation of decreasing entrapment of fines.

Several authors have noted that deposition from high-concentration turbidity currents involves the development of a laminar near-bed layer. This layer can have varying thickness depending on how fast its lower boundary with the static bed migrates upwards and how fast

sediment is supplied to its top from the flow ('traction carpet' of Sohn, 1997; 'laminar sheared layer' of Vrolijk & Southard, 1997; 'non-turbulent, concentrated basal zone' of Kneller & Branney, 1995). Vrolijk & Southard (1997) observed no significant grain fractionation in this layer and hypothesized that coarse sediment transport lag could be responsible for the development of inverse grading (Hand, 1997). However, the entrapment model is consistent with the experimental results of Vrolijk & Southard (1997). Grain-size fractionation is weak at the beginning when the shear layer is thickest and well developed. It becomes significant as the sedimentation rate declines, the shear layer thins and grains spend increasing amounts of time in it (Fig. 17b). Vrolijk & Southard (1997) observed progressive thinning of the shear layer through upward freezing of sediment in all experiments. Elutriation by escaping water can also contribute to the removal of fines. Thus, there is no need for waxing flow hydrographs (Kneller, 1995; Mulder & Alexander, 2001), complex evolution of near-bed dispersive pressure effects (Sohn, 1997) or large coarse-sediment transport lag (Hand, 1997) to explain the thick inversely graded S<sub>3</sub> division of TB1. None of these interpretations has implications that would explain the other well-developed textural trends associated with the

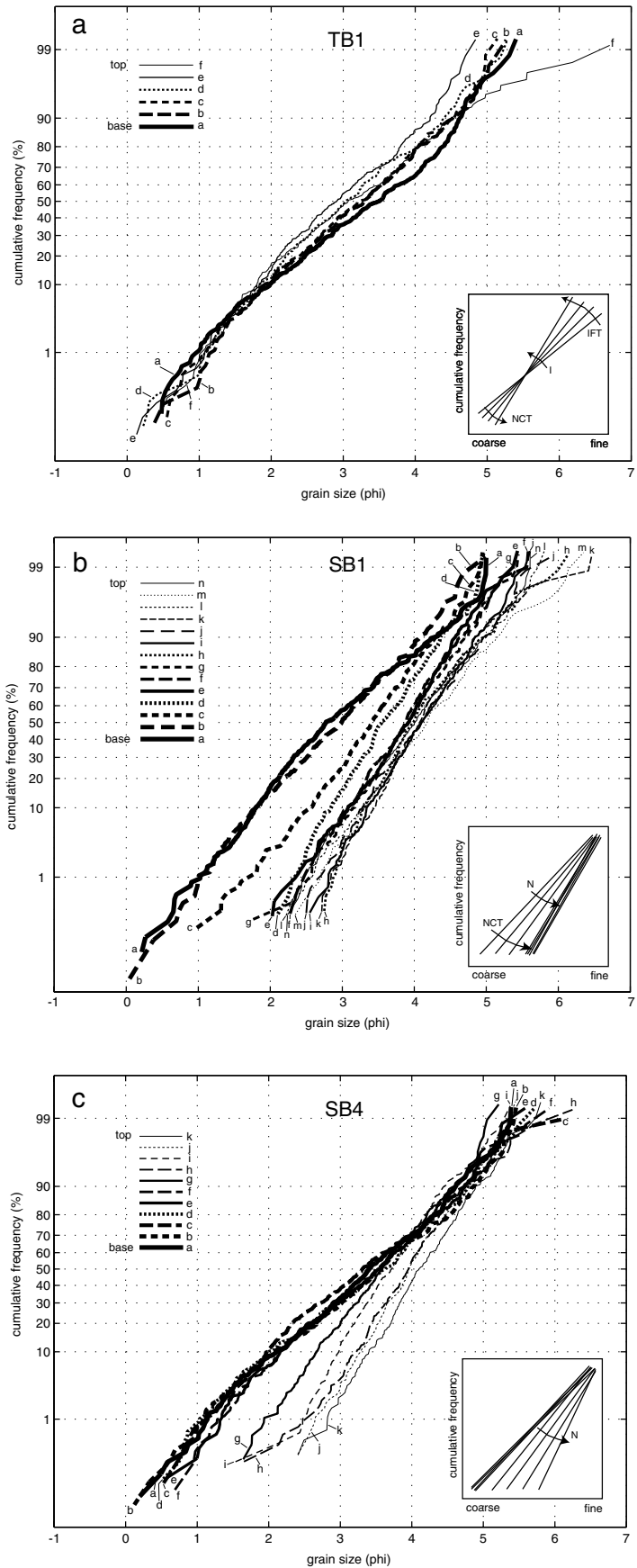


**Fig. 16.** Cumulative probability plots of grain-size data representative of different bed types. Thickness of lines decreases from the basal sample upward. (a) Bed TB1, showing inverse fine-tail grading and inverse grading in the mean. There is no mud-rich interval in this bed. (b) SB1, showing normal grading through most of its thickness, with a mud-rich division between fine-grained cross-laminated intervals. (c) SB4, with only normal coarse-tail grading in its lower, mud-rich part and normal grading in its upper part.

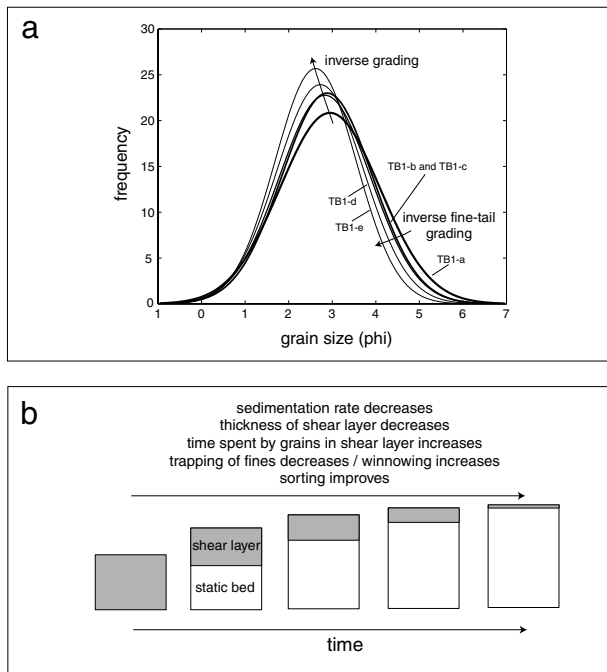


**Fig. 17.** (a) Normal fit curves of the grain-size distributions from the  $S_3$  division of TB1. For location of samples, see Fig. 12. (b) Sketch of evolution of a laminar sheared layer at the base of a high-density turbidity current and the associated trends during the depositional stage of the flow. As the sedimentation rate decreases, the thickness of the shear layer and trapping of fines decrease. Based in part on experimental observations by Vrolijk & Southard (1997).

inverse grading. One could argue that an increasing velocity can also lead to an improvement in the sorting ability of the flow. However, the difference in the mean grain sizes of the bottom (0.13 mm) and the top (0.165 mm) of the  $S_3$  division is minor.

Inverse grading is common in fluvial flood deposits (Osterkamp & Costa, 1987; Iseya, 1989; Rubin *et al.*, 1998). During the 1996 controlled flood of the Colorado River, inversely graded sand layers were deposited during steady discharge as a result of decreasing sediment concentrations in the current and increasing winnowing (Rubin *et al.*, 1998). The depositional rates were much lower than in the case of TB1, and the deposited sedimentation unit consisted of climbing ripples overlain by cross-bedding.

### Inverse fine-tail grading

The few existing textural studies of turbidites give little attention to the fine tail. Fine-tail inverse grading probably indicates decreasing entrapment of fines and increasingly competence-dom-

inated deposition with decreasing rates of suspended-load fallout. In TB3, SB3 and SB4 (Figs 12–14 and 16), the upward reduction in trapping of fines was not strong enough to result in inverse grading of the mean grain size.

### Ungraded divisions

Although rarely documented quantitatively, it seems that thick divisions of ungraded sand lacking traction structures are not uncommon in deep-water clastic successions (Dzulynski *et al.*, 1959; Leszczynski, 1989; Haines *et al.*, 2001). One possibility is that such units represent deposits of sustained, quasi-steady flows (Kneller & Branney, 1995; Haines *et al.*, 2001). However, experimental results (Middleton & Neal, 1989; Vrolijk & Southard, 1997) suggest that thick, ungraded layers are deposited from flows with the highest sediment concentrations in areas where sedimentation rates are the highest. The ungraded interval of SB3 (Fig. 13) is characterized by a slightly higher mud content than the typical  $T_a/S_3$  divisions (TB1, TB2, TB3), and it has a bipartite structure: a lower, slightly coarser and less muddy layer, separated by a parting surface from the overlying more mud-rich unit. This structure is comparable to SB4 and SB5 (Fig. 14), as well as to experimental deposits of sediment gravity flows described as weakly and moderately coherent flows by Marr *et al.* (2001). It is likely that the lower parts of SB3 and SB4 were deposited by flows that had turbulent heads but partly laminar and weakly to moderately cohesive bodies during their depositional stage. However, subtle but statistically significant vertical trends are present in both SB3 (inverse fine-tail grading and improvement in sorting) and SB4 (coarse-tail grading), and it is likely that turbulence was stronger during their main transport phase than after deposition started.

### Normal grading

Normal grading can be interpreted as reflecting tailward fining of the flow (Kuenen & Menard, 1952; Kneller & Buckee, 2000) or grain-size segregation during suspension sedimentation (Lowe, 1982). Strong longitudinal gradients of concentration and grain size can develop in surge-like turbidity currents that transport sediment over large distances. Coarse-tail normal grading has been observed to form through settling of coarser grains through the basal, non-turbulent layer (Marr *et al.*, 2001). In contrast,

well-developed normal distribution grading in  $T_{bcde}$  units is likely to reflect longitudinal flow structure.

### 'Coarse tops'

Relatively coarse-grained, parallel-laminated or cross-bedded units capping  $S_3/T_a$  divisions probably reflect the presence of energetic, high-velocity turbidity currents remaining after deposition of the coarser grained sediment loads. By this time, the suspended-load fallout rates have declined significantly, but flow velocities are still relatively high. These low-density currents rework and winnow the upper parts of the underlying  $S_3$  units, depositing current-structured  $T_t$  divisions of Lowe (1982).

### Mud-rich sandstones

The development of mud-rich divisions seems to be limited to certain stages of deposition from the flows. This stage either corresponds to the transition from the  $T_a/S_3$  division to the traction-structured parts of a turbidite or is associated with very fine-grained  $T_c$  divisions. The coarser grained and finer grained muddy sands correspond to different depositional processes.

#### *Coarser grained mud-rich sandstones*

In a 'normal' turbidity current, when rapid deposition of sand-sized sediment begins due to decreasing capacity of the flow, some mud flocs will also get deposited. However, the mud concentration in the near-bed shear layer is not high enough to result in strong cohesiveness. The flocs are not hydrodynamic equivalents of the modal sand size: they belong to the fine tail of the distribution in suspension, and high suspended-load fallout rates are needed to prevent the flocs from returning into suspension from the near-bed layer. If flow velocity is relatively high, and the sedimentation rate is decreasing, deposition becomes more and more competence driven, sorting improves and fines are removed.

A different scenario for deposition of the  $T_a/S_3$  unit results if the current is more mud rich and the suspended-load fallout rate stays high. As the grain-size distribution of the suspension shifts towards finer grain sizes, the relative amount of mud flocs in the suspension increases. Owing to high sediment concentration in the lower part of the flow and high sedimentation rates, fines are trapped in the resulting deposit. Based on experimental results, Middleton & Neal (1989) have

suggested that trapping of fines in turbidites is possible at high sediment concentrations and high sedimentation rates, but no fines would be trapped at concentrations less than 4%. The results of the present study suggest that, at a critical value of mud content, which seems to correspond to about 15% volume concentration of mud in the compacted sediment, the near-bed shear layer becomes cohesive. A distinct rheological interface develops between this cohesive layer and the overlying turbulent flow. The cohesiveness of the mud-rich layer prevents mixing with and reworking by the overlying turbulent current. These processes can result in the relatively sharp breaks in mud contents and grain sizes in some of the sedimentation units.

The slurry beds in outcrop B consist of a lower, coarser grained layer of lower mud content that seems to consist of a few dark and light bands, which passes upwards into a higher mud content and poorly sorted unit containing mud clasts (Figs 10a and 11). The upper parts of these units might have moved long distances as cohesive debris flows, as suggested by the sharp grain size and clear parting surface at their bases, the lack of grading and the slight upward decrease in the standard deviation (Fig. 14). This upward deterioration in sorting is not present in any of the mud-rich sandstones of outcrop A and suggests deposition through downward freezing of a rigid plug at the top of the flow.

#### *Finer grained mud-rich sandstones*

One of the key observations for the interpretation of the finer grained mud-rich sandstones described here is that some mud-rich intervals occur interlayered with low-mud turbidite divisions (Fig. 4a). In SB1 and SB3, normal grading in the upper 25 cm of the sedimentation unit continues uninterrupted through the mud-rich division. The upward improvement in sand sorting is also continuous through the muddy unit. However, the mud content increases abruptly in the mud-rich division. Many sedimentation units in outcrop A have several cross-laminated divisions interbedded with fine-grained muddy sandstone (Fig. 8c and d). There is no sharp grain-size break between the  $T_c$  units and the muddy divisions. This repeated interbedding of mud-rich and less muddy sandstone within the same sedimentation unit suggests that minor changes in flow properties could trigger the deposition of either mud-rich or mud-poor sand. The autocyclic behaviour of the flow resembles the dark and light band formation described by Lowe & Guy (2000). The

transition from a relatively mud-poor to a mud-rich division is probably associated with a reduction or suppression of turbulence in the near-bed part of the flow.

## DISCUSSION

### Duration of deposition of S<sub>3</sub>/T<sub>a</sub> divisions

A potential explanation for the upward-decreasing fines content in most S<sub>3</sub>/T<sub>a</sub> divisions of turbidites in the Fusaru Sandstone is that the sedimentation rate rapidly reached high values as sedimentation began and then declined gradually during sedimentation (cf. Allen, 1991). This supports the inference that sand-rich, high-density turbidity currents are sensitive to minor changes in flow parameters and, once deposition starts, a feedback mechanism leads to the collapse of a significant part of the sediment load (Lowe, 1982). Such a current does not stop instantaneously, and it does not deposit its sediment load en masse. More dilute parts of the current may bypass but rework the upper part of the sandy deposit, resulting in the well-sorted T<sub>t</sub> division of Lowe (1982) in some beds. Parker *et al.* (1987) observed that flows can even accelerate during and after significant deposition occurs.

Reasonable estimates of flow duration at individual points along the flow path can be found using the methodology of Allen (1991; see also Baas *et al.*, 2000). This approach will be used here to estimate the sedimentation rate and duration of deposition in the case of the 300 cm thick TB1 (Fig. 12), with emphasis on the massive lower part of the bed. A minimum estimate of sedimentation rate necessary to suppress the development of horizontal lamination in fine sand is about 0.67 mm s<sup>-1</sup> based on experimental (Arnott & Hand, 1989) and theoretical (Allen, 1991) constraints. This sets the maximum possible duration of deposition to about 1 h for this 240 cm thick division in TB1. However, the upward-increasing removal of fines suggests that the deposition rate was highest at the base of the bed and was declining during deposition. Although the relationship between sediment concentration and deposition rate is non-linear (e.g. Talling, 2001), in order to calculate upper and lower limits for sedimentation rates and the duration of deposition, it is assumed here that this decline is linear (cf. Allen, 1991). The equation of the depositional rate  $R$  as a function of height  $y$  above base of the bed is given by

$$R = R_0 - ky \quad (3)$$

where  $R_0$  is the initial sedimentation rate and  $k$  is the slope of the line (Allen, 1991).

As the co-ordinates ( $y$ ,  $R$ ) of two points on this line, (3.0, 0), corresponding to the top of the bed, and (2.4,  $6.7 \times 10^{-4}$ ), representing the T<sub>a</sub>/T<sub>t</sub> transition, are known,  $k$  and  $R_0$  can be calculated. The minimum initial sedimentation rate is 3.3 mm s<sup>-1</sup>. As  $R = dy/dt$ , using Eq. (3), the duration of deposition for the whole bed would be

$$t = \int 1/(R_0 - ky) dy \quad (4)$$

which results in a maximum value of about 95 min. However, the 240 cm thick S<sub>3</sub> division is deposited in only 24.5 min. If the sedimentation rate is assumed to approach zero at the boundary between the T<sub>t</sub> division and the overlying fine-grained T<sub>de</sub> unit (Fig. 18), an estimate of the maximum sedimentation rate is obtained from the two points with the ( $y$ ,  $R$ ) co-ordinates (2.65, 0) and (2.4,  $6.7 \times 10^{-4}$ ). Using Eq. (4), the S<sub>3</sub> and T<sub>t</sub> divisions are deposited in  $\approx 38$  min, out of which 15 min represent the time necessary for the deposition of S<sub>3</sub>. Thus, the initial sedimentation rate for this turbidite was probably in the range of 3.3–7.1 mm s<sup>-1</sup>, and deposition of the 240 cm thick massive sandy unit took from 15 to 25 min. In the experiments of Vrolijk & Southard (1997), sedimentation rates were as high as 20 mm s<sup>-1</sup>. This suggests that suspended-load fallout rates can be extremely high at the beginning of sedimentation. Thus, it is not unlikely that the S<sub>3</sub> division of TB1 was deposited in only a few minutes.

A more sustained turbidity current could have deposited a massive sandy unit of the same thickness in about 1 h, as pointed out above. Thus, the theoretically possible range of durations for deposition can cover a range from a few minutes to about 1 h.

### Implications for reservoir characterization

The textural properties and the presence of mud in the deep-water facies types described here will strongly influence the porosity and permeability distribution in a hydrocarbon reservoir. The laterally extensive mud-rich sandstone layers can significantly increase reservoir heterogeneity by forming flow baffles and/or barriers (see also Lowe & Guy, 2000; Haughton *et al.*, 2003; Lowe

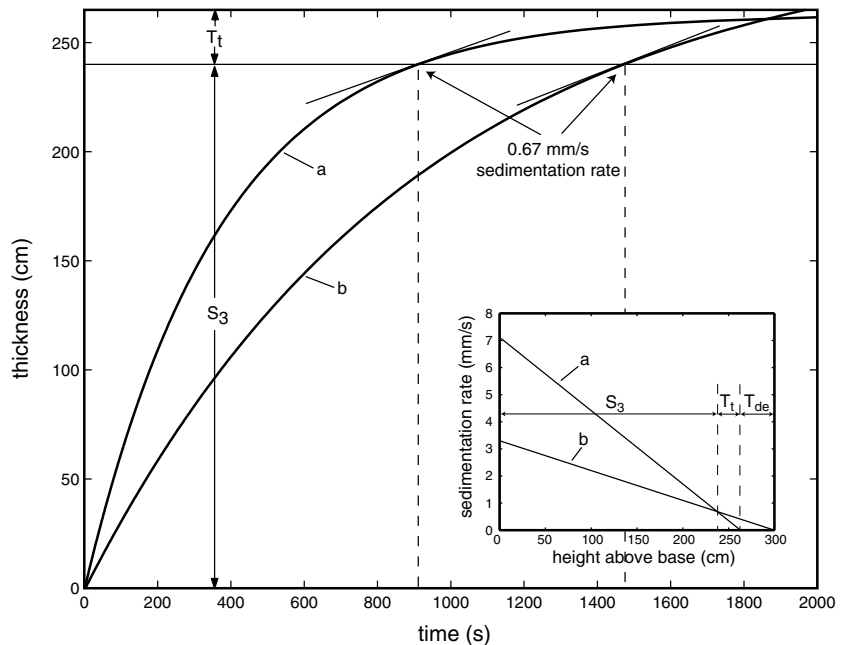


**Fig. 18.** Plot of bed thickness vs. time and sedimentation rate vs. height above base (inset) for turbidite TB1, assuming a linearly decreasing sedimentation rate and two slightly different cases: (a) sedimentation rate approaches zero at the top of the  $T_t$  division or (b) at the top of the  $T_{de}$  division. Sedimentation rate must be  $\approx 0.67 \text{ mm s}^{-1}$  at the transition between the  $S_3$  and the  $T_t$  units.

*et al.*, 2003). Furthermore, the presence of an upward improvement in sorting and inverse grading in the fine tail might be a more widespread feature of thick-bedded deep-water sandstones. In some of the thickest sandstone beds, consisting of thick  $S_3$  units, the porosity will be lowest at the base of the bed and will increase gradually upwards, in parallel with the improvement in sorting. Similarly, thinner bedded, typical Bouma  $T_a$ - and  $T_b$ -dominated turbidites will have on average higher porosities compared with the thick  $S_3$ -dominated beds (e.g. Sullivan *et al.*, 2003).

On the other hand, the presence of thick sand beds with subtle inverse grading and potential cross-bedding at their top are likely to be characteristic of more proximal depositional settings, where depositional rates are initially high but are decreasing rapidly, and there is significant bypass. Therefore, such features could be used to predict the presence of considerable sandy deposits downstream.

## CONCLUSIONS

Mud-poor and mud-rich sandy sediment gravity-flow deposits of the Oligocene flysch of the East Carpathians show subtle but statistically significant vertical grain-size trends.  $T_a/S_3$  divisions deposited by high-density turbidity currents tend to show coarse-tail normal grading and fine-tail inverse grading. The mean grain size can be

normally or inversely graded or can lack grading. Sorting improves upwards in normally and inversely graded units and shows less significant changes in ungraded intervals. Vertical grain-size trends in  $T_{bcde}$  deposits are better developed than in  $T_a/S_3$  divisions or in mud-rich units.

Similar textural trends have been observed in other ancient successions and in experimental deposits of decelerating suspension currents (e.g. Middleton, 1962; Gonzalez-Bonorino & Middleton, 1976; Hiscott & Middleton, 1980; Vrolijk & Southard, 1997; Table 2). It is suggested here that the fine-tail inverse grading, which can lead to inverse grading in the mean size as well, results from the decreasing effectiveness of entrapment of fines by the deposit as the rate of deposition declines. Figure 19 illustrates these differences with idealized changes in the shapes of normal distributions of phi grain-size measures from the base to the top of structureless sands.

With relatively high flow velocities, initially high but rapidly declining suspended-load fallout rates result in  $S_3$  divisions that are inversely graded in the mean grain size. Such beds commonly show a well-sorted, current-structured  $T_t$  unit at the top (Fig. 19a). With the same flow velocities but high suspended-load fallout rates that decline relatively slowly, the  $S_3$  units will show subtle normal grading in the mean grain size (Fig. 19b) or will be ungraded. These conditions favour the deposition of mud floccules along with sand, sometimes resulting in mud-rich divisions at the top or in place of  $S_3$ .

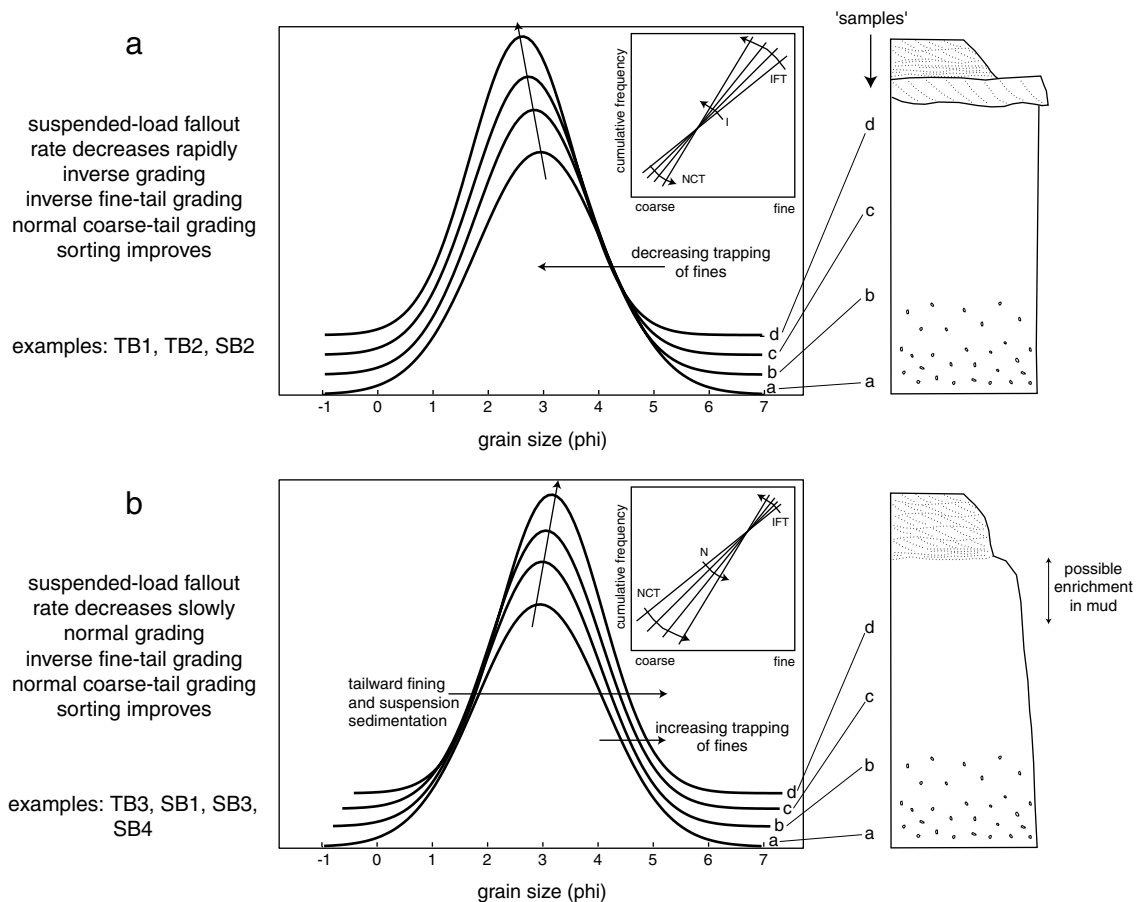


**Fig. 19.** Conceptual diagrams showing the differences between vertical textural changes in  $S_3/T_a$  deposits of rapidly depositing high-density turbidity currents. Initially high but rapidly declining suspended-load fallout rates (a) lead to upward reduction in the amount of fines trapped and winnowing of the top  $S_3$  deposits by the remaining low-density turbidity current that bypasses this location. Inverse grading in the mean grain size can result. If the suspended-load fallout rate declines more slowly (b), significant amounts of mud can be deposited with fine sand (mean grain size =  $3 \phi$  or 0.125 mm) towards the top of the  $S_3$  unit.

The presence of mud-rich sandy intervals within standard sequences of turbidite divisions suggests that most of the mud-rich units were deposited by flows that became transitional between turbidity currents and debris flows during their late-stage evolution by developing basal muddy cohesive layers. High suspended-load fallout rates created conditions for enhanced trapping of fines in coarser grained units lacking traction structures. The finer grained mud-rich units interbedded with mud-poor cross-laminated sandstone were also deposited during periods of high suspended-load fallout. In this case, the mud floccules were hydrodynamically equivalent to very fine sand or silt. Dampening of turbulence in the lower parts of the flows prevented ripple formation and floc disaggregation, resulting in fine-grained, mud-rich sandy units with a weak horizontal lamination.

This study suggests that detailed textural analysis of individual sediment gravity-flow deposits can provide information about late-stage flow evolution and depositional processes. Although sediment gravity-flow deposits of the East Carpathian Oligocene flysch have a wide variety of textural and structural trends, the subtle grading styles and trends in sorting and mud content are regular and probably reflect flow evolution that depends mainly on how rapidly sediment is falling out of the current relative to flow power and near-bed shear stress: in other words, changes in rates of sediment deposition. Vertical grain-size trends in thick-bedded deep-water sands should not be used as proxies for changes in flow velocity. Changes in suspended-load fallout rate and the related deposition or bypass of fine-grained sediment are more important than velocity fluctuations in determining the texture of the deposit.

## ACKNOWLEDGEMENTS

This study was supported by the Stanford Project on Deep-water Depositional Systems (SPODDS). Contributing industry members include Anadarko, BP, Chevron, Conoco, ENI-AGIP, Exxon-Mobil, JNOC, Marathon, Occidental, Perez Companc, Petrobras, Rohöl-Aufsuchungs AG, Shell, Texaco and Unocal. Additional funding was provided by the Stanford School of Earth Sciences Dorothea McGee Fund and Soros Foundation Romania. We are grateful to Steve Graham, Bill Normark and Tom Hickson for discussions. The careful reviews by Peter Talling and editor Peter Haughton have greatly improved the paper. Irene Espejo and Calum Macaulay helped with the microscopic work. Lajos Sylvester and Anikó Sándor are thanked for their support with the fieldwork.

## REFERENCES

- Allen, J.R.L. (1991) The Bouma division A and the possible duration of turbidity currents. *J. Sed. Petrol.*, **61**, 291–295.
- Arnott, R.W.C. and Hand, B.M. (1989) Bedforms, primary structures and grain fabric in the presence of suspended sediment rain. *J. Sed. Petrol.*, **59**, 1062–1069.
- Baas, J.H. and Best, J.L. (2002) Turbulence modulation in clay-rich sediment-laden flows and some implications for sediment deposition. *J. Sed. Res.*, **72**, 336–340.
- Baas, J.H., van Dam, R.L. and Storms, J.E.A. (2000) Duration of deposition from decelerating high-density turbidity currents. *Sed. Geol.*, **136**, 71–88.
- Banerjee, I. (1977) Experimental study on the effect of deceleration on the vertical sequence of sedimentary structures in silty sediments. *J. Sed. Petrol.*, **47**, 771–783.
- Bouma, A.H. (1962) *Sedimentology of Some Flysch Deposits; a Graphic Approach to Facies Interpretation*. Elsevier, Amsterdam, 168pp.
- Chen, C. and Hiscott, R.N. (1999) Statistical analysis of turbidite cycles in submarine fan successions: tests for short-term persistence. *J. Sed. Res.*, **69**, 486–504.
- Contescu, L., Jipa, D., Mihailescu, N. and Panin, N. (1967) The internal Paleogene flysch of the eastern Carpathians; paleocurrents, source areas and facies significance. *Sedimentology*, **7**, 307–321.
- Davies, O.L. and Goldsmith, P.L. (1977) *Statistical Methods in Research and Production*. Longman, London, 478pp.
- Dean, A. and Voss, D.T. (1999) *Design and Analysis of Experiments*. Springer, New York, 740pp.
- Dzulynski, S., Ksiazkiewicz, M. and Kuenen, P.H. (1959) Turbidites in Flysch of the Polish Carpathian mountains. *Geol. Soc. Am. Bull.*, **70**, 1089–1118.
- Felix, M. (2002) Flow structure of turbidity currents. *Sedimentology*, **49**, 397–420.
- Fodor, L., Csontos, L., Bada, G., Gyorf, I., Benkovics, L., Jolivet, L., Horvath, F. and Seranne, M. (1999) Tertiary tectonic evolution of the Pannonian Basin system and neighbouring orogens; a new synthesis of palaeostress data. In: *Mediterranean Basins; Tertiary Extension Within the Alpine Orogen* (Ed. B. Durand), *Geol. Soc. Spec. Publ.*, **156**, 295–334.
- Gonzalez-Bonorino, G. and Middleton, G.V. (1976) A Devonian submarine fan in western Argentina. *J. Sed. Petrol.*, **46**, 56–69.
- Haines, P.W., Jago, J.B. and Gum, J.C. (2001) Turbidite deposition in the Cambrian Kanmantoo Group, South Australia. *Aust. J. Earth Sci.*, **48**, 465–478.
- Hand, B.M. (1997) Inverse grading resulting from coarse-sediment transport lag. *J. Sed. Res.*, **67**, 124–129.
- Harper, C.W., Jr (1998) Thickening and/or thinning upward patterns in sequences of strata: tests of significance. *Sedimentology*, **45**, 657–696.
- Haughton, P.D.W., Barker, S.P. and McCaffrey, W.D. (2003) ‘Linked’ debrites in sand-rich turbidite systems – origin and significance. *Sedimentology*, **50**, 459–482.
- Hiscott, R.N. (1994a) Loss of capacity, not competence, as the fundamental process governing deposition from turbidity currents. *J. Sed. Res.*, **A64**, 209–214.
- Hiscott, R.N. (1994b) Traction-carpet stratification in turbidites; fact or fiction?. *J. Sed. Res.*, **A64**, 204–208.
- Hiscott, R.N. and Middleton, G.V. (1979) Depositional mechanics of thick-bedded sandstones at the base of a submarine slope, Tourelle Formation (Lower Ordovician), Quebec, Canada. In: *Geology of Continental Slopes* (Eds L.J. Doyle and O.H. Pilkey), *SEPM Spec. Publ.*, **27**, 307–326.
- Hiscott, R.N. and Middleton, G.V. (1980) Fabric of coarse deep-water sandstones, Tourelle Formation, Quebec, Canada. *J. Sed. Petrol.*, **50**, 703–721.
- Iseya, F. (1989) Mechanism of inverse grading of suspended load deposits. In: *Sedimentary Facies in the Active Plate Margin* (Eds A. Taira and F. Masuda), pp. 113–129. Terra Scientific Publishing, Tokyo.
- Johnson, M.R. (1994) Thin section grain size analysis revisited. *Sedimentology*, **41**, 985–999.
- Kneller, B.C. (1995) Beyond the turbidite paradigm; physical models for deposition of turbidites and their implications for reservoir prediction. In: *Characterization of Deep Marine Clastic Systems* (Eds A.J. Hartley and D.J. Prosser), *Geol. Soc. Spec. Publ.*, **94**, 31–49.
- Kneller, B.C. and Branney, M.J. (1995) Sustained high-density turbidity currents and the deposition of thick massive sands. *Sedimentology*, **42**, 607–616.
- Kneller, B.C. and Buckee, C. (2000) The structure and fluid mechanics of turbidity currents; a review of some recent studies and their geological implications. *Sedimentology*, **47** (Suppl. 1), 62–94.
- Komar, P.D. (1985) The hydraulic interpretation of turbidites from their grain sizes and sedimentary structures. *Sedimentology*, **32**, 395–407.
- Kranck, K. (1984) Grain-size characteristics of turbidites. In: *Fine-Grained Sediments; Deep-Water Processes and Facies* (Eds D.A.V. Stow and D.J.W. Piper), *Geol. Soc. Spec. Publ.*, **15**, 83–92.
- Kuenen, P.H. (1966) Matrix of turbidites; experimental approach. *Sedimentology*, **7**, 267–297.
- Kuenen, P.H. and Menard, H.W. (1952) Turbidity currents, graded and non-graded deposits. *J. Sed. Petrol.*, **22**, 83–96.
- Kuenen, P.H. and Migliorini, C.I. (1950) Turbidity currents as a cause of graded bedding. *J. Geol.*, **58**, 91–127.
- Kuenen, P.H. and Sengupta, S. (1970) Experimental marine suspension currents, competency and capacity. *Geol. Mijnbouw*, **49**, 89–118.
- Legros, F. (2002) Can dispersive pressure cause inverse grading in grain flows? *J. Sed. Res.*, **72**, 166–170.

- Leszczynski, S.** (1989) Characteristics and origin of fluxoturbidites from the Carpathian Flysch (Cretaceous-Palaeogene), South Poland. *Ann. Soc. Geol. Pol.*, **59**, 351–390.
- Linzer, H.-G., Frisch, W., Zweigel, P., Gîrbacea, R., Hann, H.-P. and Moser, F.** (1998) Kinematic evolution of the Romanian Carpathians. *Tectonophysics*, **297**, 133–156.
- Lowe, D.R.** (1976) Grain flow and grain flow deposits. *J. Sed. Petrol.*, **46**, 188–199.
- Lowe, D.R.** (1982) Sediment gravity flows. II. Depositional models with special reference to the deposits of high-density turbidity currents. *J. Sed. Petrol.*, **52**, 279–297.
- Lowe, D.R.** (1988) Suspended-load fallout rate as an independent variable in the analysis of current structures. *Sedimentology*, **35**, 765–776.
- Lowe, D.R. and Guy, M.** (2000) Slurry-flow deposits in the Britannia Formation (Lower Cretaceous), North Sea; a new perspective on the turbidity current and debris flow problem. *Sedimentology*, **47**, 31–70.
- Lowe, D.R., Guy, M. and Palfrey, A.** (2003) Facies of slurry-flow deposits, Britannia Formation (Lower Cretaceous), North Sea: implications for flow evolution and deposit geometry. *Sedimentology*, **50**, 45–80.
- Marr, J.G., Harff, P.A., Shanmugam, G. and Parker, G.** (2001) Experiments on subaqueous sandy gravity flows: The role of clay and water content in flow dynamics and depositional structures. *Geol. Soc. Am. Bull.*, **113**, 1377–1386.
- Middleton, G.V.** (1962) Size and sphericity of quartz grains in two turbidite formations. *J. Sed. Petrol.*, **32**, 725–742.
- Middleton, G.V.** (1967) Experiments on density and turbidity currents; [Part] 3, Deposition of sediment. *Can. J. Earth Sci.*, **4**, 475–505.
- Middleton, G.V.** (1993) Sediment deposition from turbidity currents. *Annu. Rev. Earth Planet. Sci.*, **21**, 89–114.
- Middleton, G.V. and Hampton, M.A.** (1976) Subaqueous sediment transport and deposition by sediment gravity flows. In: *Marine Sediment Transport and Environmental Management* (Eds D.J. Stanley and D.J.P. Swift), pp. 197–218. Wiley, New York.
- Middleton, G.V. and Neal, W.J.** (1989) Experiments on the thickness of beds deposited by turbidity currents. *J. Sed. Petrol.*, **59**, 297–307.
- Middleton, G.V. and Southard, J.B.** (1984) Mechanics of sediment movement. *SEPM Short Course*, **3**, 400pp.
- Migeon, S., Savoye, B., Zanella, E., Mulder, T., Faugères, J.-C. and Weber, O.** (2001) Detailed seismic-reflection and sedimentary study of turbidite sediment waves on the Var Sedimentary Ridge (SE France): significance for sediment transport and deposition and for the mechanisms of sediment-wave construction. *Mar. Petrol. Geol.*, **18**, 179–285.
- Mulder, T. and Alexander, J.** (2001) The physical character of subaqueous sedimentary density flows and their deposits. *Sedimentology*, **48**, 269–300.
- Osterkamp, W.R. and Costa, J.E.** (1987) Changes accompanying an extraordinary flood on a sand-bed stream. In: *Catastrophic Flooding* (Eds L. Mayer and D. Nash), pp. 201–224. Allen & Unwin, Boston.
- Parker, G., Garcia, M., Fukushima, Y. and W.** (1987) Experiments on turbidity currents over an erodible bed. *J. Hydr. Res.*, **25**, 123–147.
- Pierce, J.W. and Graus, R.R.** (1981) Use and misuses of the phi-scale; discussion. *J. Sed. Petrol.*, **51**, 1348–1350.
- Piper, D.J.W.** (1978) Turbidite muds and silts on deepsea fans and abyssal plains. In: *Sedimentation in Submarine Canyons, Fans, and Trenches* (Eds G. Kelling and D.J. Stanley), pp. 163–175. Dowden, Hutchinson & Ross, Stroudsburg.
- Rubin, D.M., Nelson, J.M. and Topping, D.J.** (1998) Relation of inversely graded deposits to suspended-sediment grain-size evolution during the 1996 flood experiment in Grand Canyon. *Geology (Boulder)*, **26**, 99–102.
- Shanmugam, G. and Moiola, R.J.** (1995) Reinterpretation of depositional processes in a classic flysch sequence (Pennsylvanian Jackfork Group), Ouachita Mountains, Arkansas and Oklahoma. *AAPG Bull.*, **79**, 672–695.
- Sohn, Y.K.** (1997) On traction-carpet sedimentation. *J. Sed. Res.*, **67**, 502–509.
- Ștefănescu, M. and Micu, M.** (1987) Flysch deposits in the East Carpathians. In: *Flysch Deposits from the Hartz, the Thuringian and Vogtlandian Slate Mountains, the Carpathians, the Balkans and the Caucasus* (Ed. M. Ștefănescu), pp. 65–69. Edit. Acad. RPR, Bucharest.
- Ștefănescu, M., Popescu, I., Ștefănescu, M., Ivan, V., Melinte, M. and Stănescu, V.** (1993) Aspects of the possibilities of lithological correlation of the Oligocene-lower Miocene deposits of the Buzău Valley. *Rom. J. Stratigr.*, **75**, 83–90.
- Stow, D.A.V. and Bowen, A.J.** (1980) A physical model for the transport and sorting of fine-grained sediment by turbidity currents. *Sedimentology*, **27**, 31–46.
- Sullivan, K.B., Campbell, J.S. and Dahlberg, K.E.** (2003) Petrofacies: enhancing the deepwater reservoir characterization effort in West Africa. *Petrophysics*, **44**, 177–189.
- Taira, A. and Scholle, P.A.** (1979) Deposition of resedimented sandstone beds in the Pico Formation, Ventura Basin, California, as interpreted from magnetic fabric measurements. *Geol. Soc. Am. Bull.*, **90**, 952–962.
- Talling, P.J.** (2001) On the frequency distribution of turbidite thickness. *Sedimentology*, **48**, 1297–1330.
- Vrolijk, P.J. and Southard, J.B.** (1997) Experiments on rapid deposition of sand from high-velocity flows. *Geosci. Can.*, **24**, 45–54.

*Manuscript received 28 June 2002;  
revision accepted 25 March 2004.*